Modified spin-wave theory and spin-liquid behavior of cold bosons on an inhomogeneous triangular lattice

Alessio Celi,[1,*] Tobias Grass,[1] Andrew J. Ferris,[1] Bikash Padhi,[2] David Raventós,[1] Juliette Simonet,[3,4] Klaus Sengstock,[3,4] and Maciej Lewenstein[1,5]

[1]*ICFO – Institut de Ciències Fotòniques, The Barcelona Institute of Science and Technology, 08860 Castelldefels, Spain*

[2]*Department of Physics and Institute for Condensed Matter Theory, University of Illinois at Urbana-Champaign, Urbana, 61801 Illinois, USA*

[3]*Institut für Laserphysik, Universität Hamburg, Luruper Chaussee 149, D-22761 Hamburg, Germany*

[4]*Zentrum für Optische Quantentechnologien, Universität Hamburg, Luruper Chaussee 149, D-22761 Hamburg, Germany*

[5]*ICREA – Institució Catalana de Recerca i Estudis Avançats, Lluis Companys 23, 08010 Barcelona, Spain*

(Received 31 March 2016; revised manuscript received 19 June 2016; published 5 August 2016)

Ultracold bosons in a triangular lattice are a promising candidate for observing quantum spin liquid behavior. Here we investigate, for such system, the role of a harmonic trap giving rise to an inhomogeneous density. We construct a modified spin-wave theory for arbitrary filling and predict the breakdown of order for certain values of the lattice anisotropy. These regimes, identified with the spin liquid phases, are found to be quite robust upon changes in the filling factor. This result is backed by an exact diagonalization study on a small lattice.

DOI: 10.1103/PhysRevB.94.075110

I. INTRODUCTION

Quantum spin liquids (QSL)s are at the center of interest of contemporary condensed matter physics and quantum many body theory (cf. Ref. [1]) for several reasons. P. W. Anderson proposed them as a new kind of insulator: a resonating valence bond (RVB) state [2]. The interest in these state was clearly stimulated by the fact that they were soon associated with high-T_c superconductivity [3]. Immediately it was realized that RVB spin liquids might exhibit topological order [4] and are related to fractional quantum Hall states [5] and chiral spin states [6].

Frustrated antiferromagnets (AFM) provide paradigm playground for RVB states and spin liquids (for the early reviews see Refs. [7–9]). The most prominent example is Heisenberg spin 1/2 model in a kagome lattice. Unfortunately, they are notoriously difficult for numerical simulations, since due to the (in)famous sign problem quantum Monte Carlo methods cannot be applied. Still, a lot of information can be extracted from exact diagonalization studies (for seminal early studies see Ref. [10]). There was a lot of effort to describe QSLs with various approximate analytic approaches, such as large N expansion [11], or appropriate mean-field theory [12,13]. These studies suggested that QSLs described by RVB states represent topologically ordered states with finite energy gap, analogous to those of the famous Kitaev's toric code model [14].

In parallel to AFM in kagome lattice, the so-called dimer model in triangular lattice was studied intensively [15]—it was also found that it is expected to exhibit a gapped RVB phase (see also Refs. [16,17]).

The first experimental indications of QSLs comes from studies of Mott insulator in the triangular lattices [18] and power-law conductivity inside the Mott gap in certain materials [19]. More recently, observations (cf. Refs. [20–22]) combine various standard and nonconventional detection methods in kagome Heisenberg AFM, including measurements of fractionalized excitations [21]. There are also reports of QSL behavior in the so-called *herbertsmithites* (cf. Ref. [23]).

Recently, great progress was achieved in numerical simulations of the gapped QSLs, based on the use 1D density matrix renormalization group (DMRG) codes, "wired" on 2D tori/cylinders. This approach allowed for better insight into the properties of the ground state of the Heisenberg AFM in the kagome lattice [24,25]. More importantly, it allowed obtaining convincing signature of its topological Z_2 nature. This was based on a numerical estimate for the so-called topological entanglement entropy (TEE)—the quantity that unambiguously characterizes topological gapped QSLs [26,27]. Calculations of TEE were earlier applied to the quantum dimer model in the triangular lattice [28] and to the Bose-Hubbard spin liquid in the kagome lattice [29]. They were extended to critical QSLs [30], toric code [31], and lattice Laughlin states [32]. Since these calculations aim at the subleading term in entanglement entropy, it is quite challenging to achieve good accuracy (see, for instance, Refs. [31,33]).

Recently, studies of AFM in kagome lattice were extended to novel proposals for characterizing/detecting topological excitations and dynamical structure factor [34]. Several papers discuss inclusion of the chiral terms and Dzyaloshinsky-Moriya interactions, resulting in formation of chiral QSLs [35,36]. Considerable interest was devoted also to the J_1-J_2 Heisenberg model in the kagome lattice [37] and in the square lattice [38], to the J_1-J_2-J_3 Heisenberg model in the kagome lattice [39,40], and to the Kitaev-Heisenberg model [41,42] in triangular lattices [43,44].

Systems of ultracold atoms and ions provide a very versatile playground for quantum simulation of various models of theoretical many body physics [45,46]—QSLs have in this context also quite long history. The first proposals for quantum simulators of the Kitaev model in the hexagonal lattice [47], and AFM in the kagome lattice [48–50] were formulated more than ten years ago; all of them were based on smart designs and use of superexchange interactions in optical lattices. More feasible and perhaps experimentally less demanding are proposals based on ultracold ions [51] or ultracold atoms in shaken optical lattice [52]. The latter schemes were originally

*alessio.celi@icfo.es

designed to control the value and sign of the tunneling in Bose-Hubbard models—for original theory proposal see [53], and for the first experiments in the square lattice see Ref. [54]. They should be regarded as specific examples of generation of synthetic gauge fields in optical lattices [46,55], or more precisely synthetic gauge fields in periodically driven quantum systems [56].

Change of sign of tunneling in the triangular lattice is known to be equivalent of the introduction of the π-flux synthetic "magnetic" field in the Bose-Hubbard model [5,52]. In the hardcore boson limit, one obtains then an XX AFM model in the triangular lattice, which for isotropic bonds is known to have a planar Néel ground state. If, however, the bonds are anisotropic and their values $t_1, t_2 = t_3 = t\, t_1$ can be controlled, then as the anisotropic parameter t goes from infinity to zero the model interpolates between an AFM in a rhombic lattice (with the conventional Néel ground state) to an AFM in the ideal triangular lattice (with the planar Néel ground state), and finally to an AFM in an array of weakly coupled 1D chains (with the conventional Néel ground state again). Exact diagonalizations and tensor network states simulations (PEPS) indicate that between these three Néel phases there exists two quite extended regions of gapped QSLs [51].

Interestingly, the presence and the location of the QSL phases can be determined quite accurately using the generalized spin wave theory, which signals instability at the QSL boundaries [51,57]. The spin wave method is impressively powerful and has been generalized and applied to frustrated bosons and Heisenberg model with completely asymmetric triangular lattice [58,59].

We should stress that the proposal of Ref. [52] is in principle very promising, since it requires temperature of order of $(t/U)U \simeq t$, which is achievable in realistic experimental conditions, here U denotes atom-atom on site interaction energy. In fact, initial experiment demonstrated feasibility of the scheme, but were conducted far from hardcore boson limit. In these experiments, a triangular array of cigar shaped Bose-Einstein condensates was realized, corresponding to a frustrated quasiclassical AFM [60], described by a classical XX spin model with the U(1) symmetry, and Gaussian Bogoliubov-de Gennes quantum, or better to say quasiclassical fluctuations. In the further works, by exploiting control over the temporal shape of the periodic modulation, one could realize arbitrary Peierl's phases, i.e., arbitrary fluxes of the synthetic "magnetic" field through the elementary plaquette of the lattice (Ref. [61], see also Ref. [62]). This allowed for realization of a quasiclassical spin model with competing U(1) and Ising Z_2 symmetries [63]. The route toward the strongly correlated regime and hardcore limit seem to be obscured, however, by uncontrolled heating mechanisms, most probably intrinsically associated with the periodic modulation scheme [56].

Even if this difficulty is overcome, another experimental aspect might prevent the observation of QSLs in such systems. Indeed, the overall harmonic trapping of the atomic ensemble leads to a nonconstant filling factor over the optical lattice. We should expect thus a formation of a wedding cake structure, formed by the different quantum phases (cf. Ref. [46] and references therein). How does the phase diagram look like or change in the presence of such "experimental imperfections"? This is the question we want to answer in this paper. To this aim, we apply exact diagonalization on small lattices with open and periodic boundary conditions. On large lattices, we apply modified spin-wave theory, adopted to the spatially inhomogeneous situation, which turns out to be technically much more demanding than the one pertaining to the spatially homogeneous lattice with half-integer filling. Specifically, we derive for the first time a modified spin-wave theory that works for generic homogeneous filling, which allows to study large weakly trapped systems in local density approximation. Our work provides a starting point for the future applications of tensor network state approaches like the projected entangled pair states (PEPS) to a moderate size lattices. These future calculations will aim at estimations of topological entropy, which, so far, for the considered model in the triangular lattice has not yet been accomplished even in the spatially homogeneous case with periodic boundary conditions. Studying the influence of the spatial inhomogeneities, induced by the presence of the trap or disorder, on topological entanglement entropy is a fascinating question in itself—it goes, however, beyond the scope of the present paper. While inhomogeneity due to confinement are instrinsict to ultracold atoms, our approach may be also relevant for searching QSLs in other quasi-2D condensed matter systems that present residual magnetization or inhomogeneities, for instance, due to the presence of a substrate.

The paper is structured in the following way: after introducing the system and model in Sec. II, we construct the modified spin wave theory in Sec. III. From this theory, we obtain a phase diagram in Sec. IV. In Sec. V, we consider small systems ($N \leqslant 24$) using exact diagonalization. The main conclusion drawn from our study, summarized in Sec. VI, regards the co-existence of spin liquid behavior at different filling factors smaller than $1/2$. Thus the spin liquid phase is expected to be robust against inhomogeneities due to a trapping potential. Our finding should facilitate the experimental observation of spin liquids in optical lattice systems.

II. DESCRIPTION OF THE ATOMIC MODEL AND MAP TO THE SPIN MODEL

Ultracold bosons in deep optical lattices are very well described by the Bose-Hubbard model. Therefore we will take the Bose-Hubbard Hamiltonian as a starting point for our analysis:

$$\hat{H} = \sum_{\langle ij \rangle} t_{ij}(\hat{b}_i^\dagger \hat{b}_j + \text{H.c.}) + \frac{U}{2}\sum_i \hat{n}_i(\hat{n}_i - 1) + \sum_i V_i \hat{n}_i. \tag{1}$$

Here, the $\hat{b}_i^\dagger$ and $\hat{b}_i$ are the creation and annihilation operators, respectively, at the site i of the triangular lattice, and $\hat{n}_i = \hat{b}_i^\dagger \hat{b}_i$ is the number operator of the Fock space. The first term is a possibly anisotropic nearest-neighbor hopping, with tunneling amplitudes t_{ij}. In the standard case, one would have a minus sign in front of the tunneling term. However, it is possible to control the sign (or even phase) of the tunneling, which is a crucial ingredient to generate frustration in the triangular lattice. As here we will exclusively be interested in such a scenario of reversed hopping amplitude, we absorbed the sign in the definition of t_{ij}, such that standard hopping would

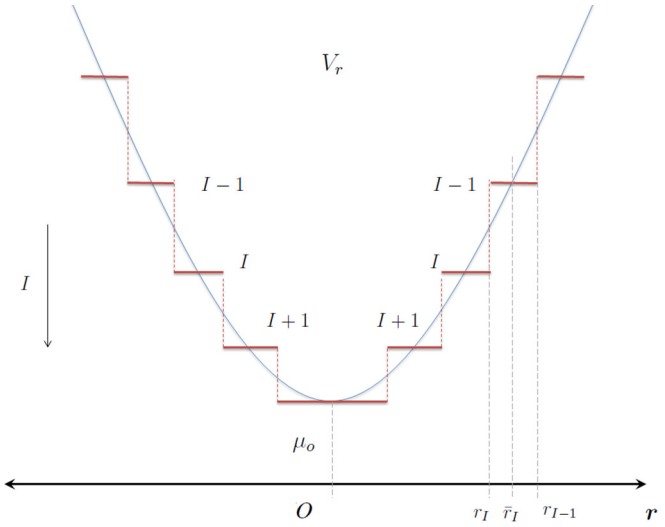

FIG. 1. Local density approximation. The harmonic potential, which for simplicity we assume to have cylindrical symmetry, is decomposed in two contributions: a steplike profile and a smoothly varying term. Each plateau extends between the radii r_I and r_{I-1}, defined as the distances where the average occupation takes two consecutive integer values, $\langle \hat{n}_{r_I} \rangle = I$, $\langle \hat{n}_{r_{I-1}} \rangle = I-1$. The hight of the plateau is taken to be the one corresponding to half-filling. The smooth terms can be then treated as a perturbation, on the same footing as the hopping term. The effective model in each plateau is thus equivalent to an anisotropic XX-spin model with a smoothly varying magnetic term.

correspond to $t_{ij} < 0$, while we will consider $t_{ij} > 0$. The second term in H describes repulsive on-site interactions of strength $U > 0$. The last term is the trapping potential $V_i = V r_i^2 - \mu_0, V = \frac{1}{2} m\omega^2$. Although it is present in any realistic experiment, it is often neglected in theoretical studies. The positions of a boson on site i is denoted by r_i.

If interactions U are strongly repulsive, fluctuations in particle number are suppressed. It is then justified to restrict the local Hilbert space to a subspace formed by the states with occupation number two. These states may change throughout the trap, but within a local density approximation, we may keep them fixed within a circular area in the center of the trap, and ring-shaped areas further outside, as illustrated in Fig. 1. Each region is denoted by an integer I, according to the possible occupation within the region, $n_I = \{I-1, I\}$.

This approach allows to map the Bose-Hubbard Hamiltonian onto a spin model, using a Holstein-Primakoff transformation [64]. Within each region I, the transformation is defined as

$$\hat{S}_i^z = (-1)^I \left(I - \frac{1}{2} - \hat{n}_i \right),$$
$$\hat{S}_i^+ = \frac{(\hat{b}^\dagger)^I}{\sqrt{I}}, \quad \hat{S}_i^- = \frac{(\hat{b})^I}{\sqrt{I}}, \quad (\hat{b}^\dagger)^2 = (\hat{b})^2 = 0. \tag{2}$$

The vanishing of squared creation or annihilation operators is due to the restriction of the local Hilbert space to two states. Using the definition of spin operators, the tunneling part of the original tight-binding Hamiltonian gets transformed to $I \sum_{\langle i,j \rangle} t_{ij} \hat{S}_i^+ \hat{S}_j^- + \text{H.c.}$ The interaction part transforms

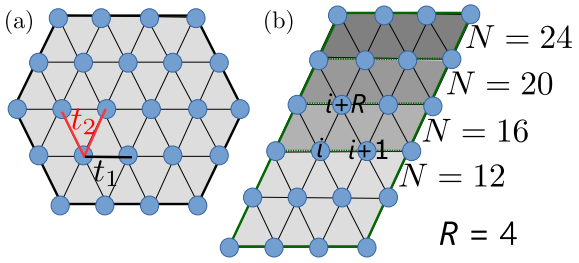

FIG. 2. (a) A triangular lattice of $N = 24$ sites with a hexagonal shape. Horizontal hopping amplitudes are given by t_1, while hopping in the other directions have an amplitude $t_2 = t\, t_1$, where t parametrizes the anisotropy of the lattice. (b) A triangular lattice of up to $N = 24$ sites with a rhombic shape. For studying the behavior upon scaling the system size (cf. Sec. V A), we use this structure. In order to conveniently define the form factor (39), the spins are identified by unique position index $i = 1, \ldots, N$, starting from the bottom left. As displayed, i increases by one while moving on the right, and by the length of the row, R, while moving up right.

to $U(\hat{S}^z)^2 + 2U(-1)^{I+1} \hat{S}_z (I-1) + U(I^2 - 2I + 3/4)$. The trap potential gives rise to a term $V_i \hat{S}_i^z$. With $(\hat{S}^z)^2 = 1/4$, and neglecting the terms that are constant within a given region I, the dynamical part of the transformed Hamiltonian is an XX model in an inhomogeneous transverse field:

$$\hat{H}_I = I \sum_{\langle ij \rangle} t_{ij} \hat{S}_i^+ \hat{S}_j^- + \text{H.c.} + \sum_i V_i \hat{S}_i^z. \tag{3}$$

Before studying this Hamiltonian in the next sections using modified spin wave theory and exact diagonalization, let us briefly discuss the parameter regimes which are of interest experimentally. As mentioned before, being interested in frustration and spin liquids, the spin-spin interactions in Eq. (3) should be antiferromagnetic, that is, $t_{ij} > 0$. To simplify the scenario, t_{ij} should only depend on the direction of the hopping, with amplitudes along horizontal links denoted t_1, while the two links with nonzero vertical component shall have an amplitude $t_2 = t\, t_1$, see Fig. 2. The anisotropy of the lattice is then characterized by a single parameter t, which we will tune from 0, corresponding to an effective 1D system, to values greater than 2, where the lattice geometry is dominated by a rhombic structure. The energy difference between neighboring spins is of the order $\Delta V_i = V a^2 \equiv \eta\, t_1$, where a is the lattice constant, and η is a dimensionless parameter. We Assume the lattice is loaded with ^{87}Rb atoms, which has lattice constant $a = 553$ nm and a trap frequency $\omega = 2\pi \times 40$ Hz; we have $\Delta V_i/\hbar = 15$ Hz. This is about an order of magnitude weaker than typical interactions strengths, $t_1/\hbar \approx 150$ Hz. In the modified spin wave approach, we will therefore take $V_i = 0$, while the effect of nonzero values will be addressed within the exact diagonalization study.

III. MODIFIED SPIN-WAVE THEORY

Let us start by analyzing the spin system for constant *nonzero* magnetization, which corresponds to fillings different from $\frac{1}{2}$. Classically, we expect the spin oriented along a cone around the z axis,

$$\mathbf{S}_i = (\sin\rho\, \cos(\mathbf{Q}\cdot\mathbf{r}_i), \sin\rho\, \sin(\mathbf{Q}\cdot\mathbf{r}_i), \cos\rho). \tag{4}$$

Here, $\boldsymbol{Q} = (Q_x, Q_y)$ is a vector in the xy plane, while ρ is the azimuthal angle related to the magnetization along the z axis, i.e., to the filling of the original bosons $\nu = \langle \hat{n} \rangle - [\langle \hat{n} \rangle]$, where $[x]$ = integer part of x. For $\rho = \frac{\pi}{2}$, (4) reduces to the ansatz considered by Refs. [57,65] at half-filling. If we follow the standard spin-wave approach, we should choose the local basis in such a way that the new local z axis is parallel to the vector (4). In this way, by applying the bosonization of the local spin we would model fluctuations *along the classical ordering* represented by (4). Now, such fluctuations would have a component also along the z axis. In other words, they would renormalize the filling factor. Such behavior is not acceptable from the physical point of view. Indeed, in the original bosonic Hubbard model, the filling factor is a well defined quantity: the hopping term conserves the particle number, and, thus, the expectation value of the particle density which is the filling. The same argument holds for the same physical model as described as a spin system. In practice, the acceptable fluctuations are restricted to the xy plane, and, precisely, are along the projection of the ordering vector on the xy plane. That is to say that a corrected choice for the quantization axis is the same as at half-filling.

What is then the difference with respect to the half-filling case? The difference resides in the magnitude of the spin projection. If we do the reasonable assumption that the fluctuations are proportional to such length we can relate n, the local density of bosonic excitations, to the filling. As originally proposed by Takahashi [66], such density at half-filling should be taken equal to the total spin, $n = S$, that to say also the bosonic excitations are at half-filling. Here, we propose a generalized Takahashi condition

$$n = S|\sin\rho|, \tag{5}$$

where the angle ρ is related to the filling by the relation $\langle S^z \rangle = \nu - S = S\cos\rho$, which implies $|\sin\rho| = \frac{1}{S}\sqrt{\nu(2S-\nu)}$. This choice has further physical justification. First, it is symmetric around half-filling as it should be: reversing the quantization axis $\hat{z}$ in the Dyson-Maleev transformation [67–69] is equivalent to the replacement $\nu \to 2S - \nu$. Second, fluctuations are maximal at half-filling and are suppressed in the paramagnetic (Mott) phases, which correspond to filling $\nu = 0$ and $2S$.

As derived in previous sections, the filling factor ν is smoothly changing in the trap and relates to the harmonic potential as $\nu = [\frac{\mu}{U} + \frac{1}{2}]$, where $[x]$ = fractional part of x (the hopping term has zero mean). Thus our analysis can be applied in local density approximation to trapped systems.

We define the local spin operators $\hat{\mathbf{S}}' \equiv (\hat{S}^{x'}, \hat{S}^{y'}, \hat{S}^{z'})$ that are related to the global ones $\hat{\mathbf{S}} = (\hat{S}^x, \hat{S}^y, \hat{S}^z)$ through the rotation

$$\hat{\mathbf{S}} = R(\theta_i)\hat{\mathbf{S}}' \equiv R(\mathbf{Q}\cdot\mathbf{r}_i)\hat{\mathbf{S}}', \tag{6}$$

where

$$R(\theta_i) = R_z(\theta_i)R_y(-\pi/2)R_z(\theta_i) = \begin{pmatrix} 0 & -\sin(\theta_i) & -\cos(\theta_i) \\ 0 & \cos(\theta_i) & -\sin(\theta_i) \\ 1 & 0 & 0 \end{pmatrix}$$

is the rotation that sends the vector $(0,0,-1)$ to $(\cos\theta_i, \sin\theta_i, 0)$, i.e., along the projection of ordering vector on the xy plane.

By composing with the Dyson-Maleev transformations

$$\begin{aligned} \hat{S}_i^{z'} &\to -S + a_i^\dagger a_i, \\ \hat{S}_i^{+'} &\to \sqrt{2S}a_i, \\ \hat{S}_i^{z'} &\to \sqrt{2S}\left(1 - \frac{a_i^\dagger a_i}{2S}\right)a_i, \end{aligned} \tag{7}$$

we find that in the original spin basis, the bosonization is

$$S_i^{\pm} = e^{\pm i\theta_i}\left\{ \pm\sqrt{\frac{S}{2}}\left[a_i^\dagger - \left(1 - \frac{\hat{n}_i}{2S}\right)a_i\right] + S\left(1 - \frac{\hat{n}_i}{S}\right)\right\}, \tag{8}$$

where $\hat{n}_i = a_i^\dagger a_i$, $\theta_{ij} = \boldsymbol{Q}\cdot\boldsymbol{r}_{ij}$, and $\boldsymbol{r}_{ij} = \boldsymbol{r}_j - \boldsymbol{r}_i$. The effective Hamiltonian reads (up to fourth order in a or $a^\dagger$)

$$\begin{aligned} H &= \frac{1}{2}\sum_{\langle ij\rangle} t_{ij}(S_i^+ S_j^- + S_i^- S_j^+) \\ &= \sum_{\langle ij\rangle} t_{ij}\cos\theta_{ij}\left(S^2 - S(\hat{n}_i + \hat{n}_j) - \frac{S}{2}(a_i^\dagger a_j^\dagger + a_i a_j) + \frac{S}{2}(a_i^\dagger a_j + a_i a_j^\dagger) + \hat{n}_i\hat{n}_j - \frac{1}{4}(a_i^\dagger \hat{n}_j a_j + a_j^\dagger \hat{n}_i a_i) + \frac{1}{4}(\hat{n}_j a_j a_i + \hat{n}_i a_i a_j)\right) \\ &\quad - i\sum_{\langle ij\rangle} t_{ij}\sin\theta_{ij}\left(S\frac{\sqrt{2S}}{2}(a_i^\dagger - a_j^\dagger - a_i + a_j) + \frac{\sqrt{2S}}{4}(\hat{n}_i a_i - \hat{n}_j a_j) - \frac{\sqrt{2S}}{2}(\hat{n}_j a_i^\dagger - \hat{n}_i a_j^\dagger - \hat{n}_j a_i + \hat{n}_i a_j)\right). \end{aligned} \tag{9}$$

Note that this expression does not coincide with Eq. (5) in Ref. [57]; indeed, the odd terms in $\sin\theta_{ij}$ are absent there as they have zero expectation value on a thermal gas of excitations. It is worth noticing that the terms in $\cos\theta_{ij}$ and $\sin\theta_{ij}$ are manifestly symmetric and antisymmetric under the exchange of indices, $i \leftrightarrow j$, respectively. Indeed, by construction the whole expression is invariant under such exchange of summed indices. Furthermore, the Hamiltonian (9) can be rewritten in an explicit translational invariant fashion by noticing that the sum over the links can be performed as a sum over there links coming out of a site, and then summing over all the sites. As these three lattice vectors on a triangular lattice we choose $\boldsymbol{\tau}_1 = (1,0), \boldsymbol{\tau}_2 = \frac{1}{2}(1,\sqrt{3}), \boldsymbol{\tau}_3 = \frac{1}{2}(-1,\sqrt{3})$. As H in Eq. (9) is non-Hermitian, following Takahashi [66], we use it in order to construct a free energy for a gas of bosonic excitations in a generic Bogoliubov basis at temperature T, i.e.,

$$\mathcal{F} = E - T\mathcal{S} + \mu(n - S|\sin\rho|), \tag{10}$$

where E is the expectation value of H,

$$E = \frac{1}{N}\sum_{\boldsymbol{k}}\langle \nu_{\boldsymbol{k}}|H|\nu_{\boldsymbol{k}}\rangle,\ \ \nu_{\boldsymbol{k}} \equiv \langle \alpha^{\dagger}_{\boldsymbol{k}}\alpha_{\boldsymbol{k}}\rangle = \frac{1}{\exp[w_{\boldsymbol{k}}/T]-1}, \tag{11}$$

with $\alpha_{\boldsymbol{k}}$ denoting the Bogoliubov modes, see Eq. (16). The entropy $\mathcal{S}$ of the bosonic gas is defined as

$$\mathcal{S} = \frac{1}{N}\sum_{\boldsymbol{k}}[(\nu_{\boldsymbol{k}}+1)\ln(\nu_{\boldsymbol{k}}+1) - \nu_{\boldsymbol{k}}\ln\nu_{\boldsymbol{k}}]. \tag{12}$$

The last term in Eq. (10) is the modified Takahashi constraint over the density of fluctuations $n = \langle \hat{n}_i\rangle$, with μ the corresponding Lagrange multiplier or chemical potential. Here, $w_{\boldsymbol{k}}$ is energy of each mode. From the functional form of the entropy it follows that $w_{\boldsymbol{k}}$ is also the rate at which the entropy changes with changing occupation, i.e., $w_{\boldsymbol{k}} = T\frac{\partial \mathcal{S}}{\partial \nu_{\boldsymbol{k}}}$.

It seems natural to adopt this strategy since the expectation value E is in general bounded from below and depends only on the average value of the bilinears $a_i^{\dagger}a_j$, $a_i^{\dagger}a_j^{\dagger}$, and their complex conjugates. This happens because the Bogoliubov transformation is by definition linear and only the quadratic bilinears above can have nonzero matrix elements while preserving the excitation number. This physical consideration is equivalent to state that E can be calculated using Wick theorem and that linear and cubic terms give zero contribution. For convenience, we define

$$\begin{aligned}\langle a_i^{\dagger}a_j\rangle &\equiv F(r_{ij}) - \tfrac{1}{2}\delta_{ij},\\ \langle a_i a_j\rangle &\equiv G(r_{ij}).\end{aligned} \tag{13}$$

In this notation, the generalized Takahashi constraint reads

$$F(0) = \langle a^{\dagger}a\rangle + \tfrac{1}{2} = S|\sin\rho| + \tfrac{1}{2}, \tag{14}$$

where $|\sin\rho|$ relates to the filling ν of the original spin system, $0 \leqslant \nu \leqslant 2S$, as $|\sin\rho| = \frac{1}{S}\sqrt{\nu(2S-\nu)}$. From (9), we find

$$\begin{aligned}\frac{E}{N} &= S^2\,C - 2S\,C\left[F(0)-\frac{1}{2}\right] - \frac{S}{2}\sum_J [c_J\cdot(G_J + G_J^* - F_J - F_J^*)]\\ &+ C\left[F(0)-\frac{1}{2}\right]^2 + \sum_J c_J(|F_J|^2 + |G_J|^2) + \frac{1}{4}c_J\left\{(G(0)(F_J + F_J^* - 2G_J^*) - 2\left[F(0)-\frac{1}{2}\right](F_J + F_J^* - 2G_J)\right\}.\end{aligned} \tag{15}$$

Here, we adopt the notation $F_J \equiv F(\tau_J)$, $G_J \equiv G(\tau_J)$, and we define $(c_1,c_2,c_3) \equiv (\cos(\boldsymbol{Q}\cdot\tau_1), t\cos(\boldsymbol{Q}\cdot\tau_2), t\cos(\boldsymbol{Q}\cdot\tau_3))$, $C \equiv c_1 + c_2 + c_3$. For convenience, we fix the energy scale such to have t_1.

If we assume that the Bogoliubov transformation is real as in Ref. [57]

$$\begin{aligned}a_{\boldsymbol{k}} &= (\cosh\theta_{\boldsymbol{k}}\,\alpha_{\boldsymbol{k}} + \sinh\theta_{\boldsymbol{k}}\,\alpha^{\dagger}_{-\boldsymbol{k}}),\\ a_{-\boldsymbol{k}} &= (\cosh\theta_{\boldsymbol{k}}\,\alpha_{-\boldsymbol{k}} + \sinh\theta_{\boldsymbol{k}}\,\alpha^{\dagger}_{\boldsymbol{k}}),\end{aligned} \tag{16}$$

we have that $F_J = F_J^*$, $G_J = G_J^*$, the expectation value of energy density reduces to

$$\begin{aligned}\frac{E}{N} = \frac{1}{2}\sum_J c_J\Bigg[&\left(S+\frac{1}{2}-F(0)+F_J\right)^2\\ &+\left(S+\frac{1}{2}-F(0)-G_J\right)^2\\ &+G(0)(F_J-G_J)+F_J^2+G_J^2\Bigg],\end{aligned} \tag{17}$$

which differs from the expression [57, Eq. (6)] not only due to the mismatch between our (9) and Eq. (5) in Ref. [57]: in fact the term $G(0)(F_J - G_J)$ is omitted as considered negligible. This approximation is justified at half-filling for large S as $F_J \sim G_J \sim S$.

It is worth noticing that the structure of the minimal solution is not affected by the explicit form of E, while the consistency equations obviously are. Indeed, due to (16), the expectation values have the form

$$\begin{aligned}F(\boldsymbol{r}) &= \frac{1}{N}\sum_{\boldsymbol{k}}\cosh(2\theta_{\boldsymbol{k}})e^{-i\boldsymbol{k}\boldsymbol{r}}\left(\nu_{\boldsymbol{k}}+\frac{1}{2}\right)\\ &= \frac{1}{N}\sum_{\boldsymbol{k}'}\cosh(2\theta_{\boldsymbol{k}'})\cos(\boldsymbol{k}'\boldsymbol{r})(2\nu_{\boldsymbol{k}'}+1),\\ G(\boldsymbol{r}) &= \frac{1}{N}\sum_{\boldsymbol{k}}\sinh(2\theta_{\boldsymbol{k}})e^{-i\boldsymbol{k}\boldsymbol{r}}\left(\nu_{\boldsymbol{k}}+\frac{1}{2}\right)\\ &= \frac{1}{N}\sum_{\boldsymbol{k}'}\sinh(2\theta_{\boldsymbol{k}'})\cos(\boldsymbol{k}'\boldsymbol{r})(2\nu_{\boldsymbol{k}'}+1),\end{aligned} \tag{18}$$

where we use explicitly the symmetry $\boldsymbol{k} \to -\boldsymbol{k}$: the prime indicates that now the sum is performed over half of the first Brillouin zone. The condition for $\mathcal{F}$ to be minimal reduces to

$$\begin{aligned}0 &= \frac{\partial\mathcal{F}}{\partial w_{\boldsymbol{k}}} = \frac{\partial\mathcal{F}}{\partial\nu_{\boldsymbol{k}}}\\ &= \sum_{\mu=0}^{3}\left[\frac{\partial E}{\partial F_\mu}\cos(\boldsymbol{k}\boldsymbol{\tau}_\mu)\cosh(2\theta_{\boldsymbol{k}}) + \frac{\partial E}{\partial G_\mu}\cos(\boldsymbol{k}\boldsymbol{\tau}_\mu)\sinh(2\theta_{\boldsymbol{k}})\right]\\ &\quad - w_{\boldsymbol{k}} + \mu\cosh(2\theta_{\boldsymbol{k}}),\end{aligned} \tag{19}$$

$$\begin{aligned}0 &= \frac{\partial\mathcal{F}}{\partial\theta_{\boldsymbol{k}}} = \frac{\partial\mathcal{F}}{2\partial\theta_{\boldsymbol{k}}}\\ &= \sum_{\mu=0}^{3}\left[\frac{\partial E}{\partial F_\mu}\cos(\boldsymbol{k}\boldsymbol{\tau}_\mu)\sinh(2\theta_{\boldsymbol{k}}) + \frac{\partial E}{\partial G_\mu}\cos(\boldsymbol{k}\boldsymbol{\tau}_\mu)\cosh(2\theta_{\boldsymbol{k}})\right]\\ &\quad + \mu\sinh(2\theta_{\boldsymbol{k}}).\end{aligned} \tag{20}$$

Here, $\boldsymbol{\tau}_0 = (0,0)$ while $\boldsymbol{\tau}_J$, $J = 1,2,3$, have been introduced above.

The condition (20) is always equivalent to

$$\tanh(2\theta_{\boldsymbol{k}}) = \frac{A_{\boldsymbol{k}}}{B_{\boldsymbol{k}}}, \tag{21}$$

and the condition (19) to

$$w_{\boldsymbol{k}} = \sqrt{B_{\boldsymbol{k}}^2 - A_{\boldsymbol{k}}^2}, \tag{22}$$

where

$$\begin{aligned}
A_{\boldsymbol{k}} &\equiv -\sum_{\mu=0}^{3} \cos(\boldsymbol{k}\boldsymbol{\tau}_\mu)\frac{\partial E}{\partial G_\mu} \\
&= \frac{1}{2}\sum_J c_J[G_J - F_J + \cos(\boldsymbol{k}\boldsymbol{\tau}_J)(1 + 2S - 2F_0 \\
&\quad + G_0 - 4G_J)] \\
&= \frac{1}{2}\sum_J c_J[G_J - F_J + \cos(\boldsymbol{k}\boldsymbol{\tau}_J)(2S(1 - |\sin\rho|) \\
&\quad + G_0 - 4G_J)], \\
B_{\boldsymbol{k}} &\equiv \mu + \sum_{\mu=0}^{3} \cos(\boldsymbol{k}\boldsymbol{\tau}_\mu)\frac{\partial E}{\partial F_\mu} \\
&= \mu + \sum_J c_J\Bigg[-2S - 1 + 2F_0 + G_J - F_J \\
&\quad + \cos(\boldsymbol{k}\boldsymbol{\tau}_J)\left(S + \frac{1}{2} + \frac{1}{2}G_0 - F_0 + 2F_J\right)\Bigg] \\
&= \mu + \sum_J c_J\Bigg[-2S(1 - |\sin\rho|) + G_J - F_J \\
&\quad + \cos(\boldsymbol{k}\boldsymbol{\tau}_J)\left(S(1 - |\sin\rho|) + \frac{1}{2}G_0 + 2F_J\right)\Bigg],
\end{aligned} \tag{23}$$

in the second lines of the expression for $A_{\boldsymbol{k}}$ and $B_{\boldsymbol{k}}$ we impose the generalized Takahashi constraint.

Thus one is getting the same result as for the diagonalization of a quartic Hamiltonian that in momentum space is real and symmetric under $\boldsymbol{k} \leftrightarrow -\boldsymbol{k}$. This can be the case when the expectation value E is real, but not otherwise.

At the formal level, we can use (21) and (22) that imply

$$\begin{aligned}
\cosh(2\theta_{\boldsymbol{k}'}) &= \sqrt{\frac{B_{\boldsymbol{k}'}^2}{B_{\boldsymbol{k}'}^2 - A_{\boldsymbol{k}}^2}}, \\
\sinh(2\theta_{\boldsymbol{k}'}) &= \frac{A_{\boldsymbol{k}'}}{B_{\boldsymbol{k}'}}\sqrt{\frac{B_{\boldsymbol{k}'}^2}{B_{\boldsymbol{k}'}^2 - A_{\boldsymbol{k}'}^2}},
\end{aligned} \tag{24}$$

to write an implicit equation for the correlation functions

$$\begin{aligned}
F(\boldsymbol{r}) &= \frac{1}{N}\sum_{\boldsymbol{k}'}\sqrt{\frac{B_{\boldsymbol{k}'}^2}{B_{\boldsymbol{k}'}^2 - A_{\boldsymbol{k}}^2}}\cos(\boldsymbol{k}'\boldsymbol{r})(2\nu_{\boldsymbol{k}'} + 1), \\
G(\boldsymbol{r}) &= \frac{1}{N}\sum_{\boldsymbol{k}'}\frac{A_{\boldsymbol{k}'}}{B_{\boldsymbol{k}'}}\sqrt{\frac{B_{\boldsymbol{k}'}^2}{B_{\boldsymbol{k}'}^2 - A_{\boldsymbol{k}'}^2}}\cos(\boldsymbol{k}'\boldsymbol{r})(2\nu_{\boldsymbol{k}'} + 1).
\end{aligned} \tag{25}$$

The following physical considerations are in order. In the zero temperature limit, we are interested in, the gas of Bogoliubov excitations is expected to condense. Such condensation is consistent with the spin ordering only if the zero mode condenses, as such condensation translates into an infinite range correlation in the original atomic system. The requirement of zero mode to become macroscopically occupied at low temperature, $M_0 = \int_{|\boldsymbol{k}|<\epsilon} \nu_k \sim Nn$, implies that $w_{\boldsymbol{k}=0} \to 0$, which also corresponds to $|\theta_{\boldsymbol{k}=0}| \to \infty$. Thus this condition can be realized only for $B_{\boldsymbol{k}=0} \sim A_{\boldsymbol{k}=0}$, which implies that in the phase we are interested in, the chemical potential has to be set to zero, $\mu = 0$. Note that this also means the occupation of each mode $\nu_{\boldsymbol{k}}$ is much smaller than $\frac{1}{2}$ (at least for $S = \frac{1}{2}$). Thus, by singling out the zero mode and using $\nu_{\boldsymbol{k}} + \frac{1}{2} \sim \frac{1}{2}$ in the expression for correlation functions, they become

$$\begin{aligned}
F(\boldsymbol{r}) &\sim M_0 + \frac{1}{N}\sum_{\boldsymbol{k}'\neq 0}\cosh(2\theta_{\boldsymbol{k}'})\,\cos(\boldsymbol{k}'\boldsymbol{r}), \\
G(\boldsymbol{r}) &\sim M_0 + \frac{1}{N}\sum_{\boldsymbol{k}'\neq 0}\sinh(2\theta_{\boldsymbol{k}'})\,\cos(\boldsymbol{k}'\boldsymbol{r}),
\end{aligned} \tag{26}$$

and the constraint (14) reads

$$M_0 + \frac{1}{N}\sum_{\boldsymbol{k}'\neq 0}\cosh(2\theta_{\boldsymbol{k}'}) = S|\sin\rho| + \frac{1}{2}. \tag{27}$$

After having singled out the zero mode and constrained the occupation the function $A_{\boldsymbol{k}}$ and $B_{\boldsymbol{k}}$ should be redefined in form accordingly. In fact only $B_{\boldsymbol{k}}$ gets redefined. Indeed, by recalculating the consistency condition for an extremum of the $\mathcal{F}$ for the new definition of the correlation functions—that to say taking into account the dependence of M_0 on $\nu_{\boldsymbol{k}}$ and $\theta_{\boldsymbol{k}}$, as well as $\mu = 0$—we have

$$\begin{aligned}
0 &= \frac{\partial\mathcal{F}}{\partial w_{\boldsymbol{k}}} = \frac{\partial\mathcal{F}}{\partial\nu_{\boldsymbol{k}}} \\
&= \sum_{\mu=0}^{3}\Bigg[\frac{\partial E}{\partial F_\mu}(\cos(\boldsymbol{k}\boldsymbol{\tau}_\mu) - 1)\cosh(2\theta_{\boldsymbol{k}}) \\
&\quad + \frac{\partial E}{\partial G_\mu}(\cos(\boldsymbol{k}\boldsymbol{\tau}_\mu)\sinh(2\theta_{\boldsymbol{k}}) - \cosh(2\theta_{\boldsymbol{k}}))\Bigg] - w_{\boldsymbol{k}},
\end{aligned} \tag{28}$$

$$\begin{aligned}
0 &= \frac{\partial\mathcal{F}}{\partial\theta_{\boldsymbol{k}}} = \frac{\partial\mathcal{F}}{2\partial\theta_{\boldsymbol{k}}} \\
&= \sum_{\mu=0}^{3}\Bigg[\frac{\partial E}{\partial F_\mu}(\cos(\boldsymbol{k}\boldsymbol{\tau}_\mu) - 1)\sinh(2\theta_{\boldsymbol{k}}) \\
&\quad + \frac{\partial E}{\partial G_\mu}(\cos(\boldsymbol{k}\boldsymbol{\tau}_\mu)\cosh(2\theta_{\boldsymbol{k}}) - \sinh(2\theta_{\boldsymbol{k}}))\Bigg].
\end{aligned} \tag{29}$$

The above equations again imply

$$\tanh(2\theta_{\boldsymbol{k}}) = \frac{A_{\boldsymbol{k}}}{B_{\boldsymbol{k}}}, \quad w_{\boldsymbol{k}} = \sqrt{B_{\boldsymbol{k}}^2 - A_{\boldsymbol{k}}^2},$$

or alternatively

$$\cosh(2\theta_{k'}) = \sqrt{\frac{B_{k'}^2}{B_{k'}^2 - A_k^2}}, \quad \sinh(2\theta_{k'}) = \frac{A_{k'}}{B_{k'}}\sqrt{\frac{B_{k'}^2}{B_{k'}^2 - A_{k'}^2}}. \tag{30}$$

The expression for A_k remains the same as in Eq. (23),

$$A_k = -\sum_{\mu=0}^{3} \cos(k\tau_\mu)\frac{\partial E}{\partial G_\mu}, \tag{31}$$

while B_k becomes

$$B_k = \sum_{\mu=0}^{3}\left[\frac{\partial E}{\partial F_\mu}(\cos(k\tau_\mu) - 1) - \frac{\partial E}{\partial G_\mu}\right]. \tag{32}$$

It is easy to check that the classical order is recovered in the limit of S large. At leading order, the minimum of the free energy is just determined by the minimum of C: the Q order found is the classical result, $Q_{Cl} = (2\arccos(-t/2),0)$, which corresponds to $(c_1,c_2,c_3) = (\frac{t^2-2}{2},-\frac{t^2}{2},-\frac{t^2}{2})$. At the next order in $\frac{1}{S}$, which corresponds to the linear spin wave (LSW) calculation, we recover the ordinary spin-wave result:

$$A_k \to S\sum_J c_J \cos(k\tau_J), \quad B_k \to S\sum_J c_J(\cos(k\tau_J) - 2), \tag{33}$$

which imply

$$w_k = 2S\sqrt{C\left(C - \sum_J c_J \cos(k\tau_J)\right)},$$

in particular $w_{k=0} = 0$ as expected. It is easy to check that, for the classical order Q_{Cl}, w_k is always real and that is by construction an extreme. In fact, as it can be checked numerically that it is also the minimal energy solution, also then the terms in $\frac{1}{S}$, which corresponds to the case in which quadratic fluctuations are included. Taking into account all the terms in Eq. (17), which include also $\frac{1}{S^2}$ corrections, known as the modified spin wave (MSW) approach, the minimum condition is no longer algebraic. As in Ref. [57], we will search for solutions recursively, starting from the ordinary spin wave solution above. The absence of a pronounced minimal value will signal the existence of a possible spin-liquid phase. In order to find the optimal $Q = (Q_x, Q_y)$, we have to impose that the gradient is zero:

$$0 = \frac{\partial \mathcal{F}}{\partial Q_x} = \sum_J \frac{\partial E}{\partial c_J}\frac{\partial c_J}{\partial Q_x},$$
$$0 = \frac{\partial \mathcal{F}}{\partial Q_y} = \sum_J \frac{\partial E}{\partial c_J}\frac{\partial c_J}{\partial Q_y}. \tag{34}$$

IV. RESULT FROM THE MODIFIED SPIN WAVE ANALYSIS

In the previous section, we have derived a modified spin wave theory for the XX-spin model on a triangular lattice. We will now extract concrete results from this theoretical framework. This amounts for a minimization problem of the free energy, which is complicated due to the large amount of variables. Using the procedure described in the subsection below, we manage to perform minimization even for large lattices with hundreds of sites. As the result, we then obtain the phase diagram for a realistic experimental system as a function of the hopping anisotropy t.

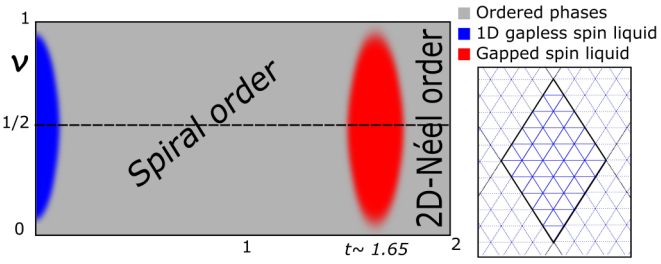

FIG. 3. Expected phase diagram as function of the filling within the MSW approach. The two ordered phases are spiral order, $0.2 \lesssim t \lesssim 1.55$, and 2D-Néel order. Inset: A 6×6 lattice of rhombic shape with periodic boundary conditions.

A. Optimization and stability

In search for a long-range order in the quartic case, we adopt an iterative procedure. We start from the ordinary spin-wave (33) solution with $Q = Q_{Cl}$ as initial configuration. The recursive procedure works as follows. First, the values of A_k, B_k at the cycle m are used to get the new correlation functions F_μ, G_μ, using Eq. (26). Once the correlations are substituted in the free energy, which at zero temperature reduces to the expectation value of the energy (17), the latter becomes a function of the ordering vector Q only, $E = E(Q)$. The new value at the cycle m of Q is, thus, determined by minimizing the $E(Q)$ in the neighborhood of optimal value of Q at the cycle m. Finally, (31) and (32) are used to update A_k and B_k as a function of the correlation functions and of the order vector. Convergence of the iterative process is assumed when the difference between the old and the updated values of A_k and B_k are below a certain threshold.

We have benchmarked the performance of this iterative approach against brute force minimization of the energy as a function of the free parameters θ_k and Q for different shapes and sizes of lattices with periodic boundary conditions. While the success and efficiency of the iterative approach, i.e., the number of iterations needed for achieving convergence, strongly depends on the shape of the lattice, it performs generally better than a brute force minimization and the scalability with the lattice size is pretty good. Best performance is achieved for rhombic lattices, see Fig. 3. Converge or failure occurs after few tens of iterations. The latter manifests when $|A_k|$ becomes greater than $|B_k|$ for some k, which corresponds to w_k becoming imaginary. In fact, more than a real instability, the absence of convergence signals that the approximation we have used of neglecting the occupation ν_k of the modes $k \neq 0$ is not respected. That is to say, the physical assumption of the existence of an ordered phase behind the spin-wave analysis is not verified. The comparison between the iterative approach and the brute force minimization of the free energy, which we

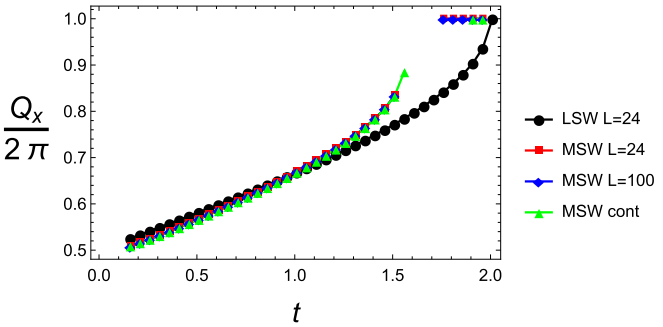

FIG. 4. Values of the optimal Q_x: comparison of results from LSW and from MSW for different sizes of the rhombic-shape lattices with periodic boundary conditions.

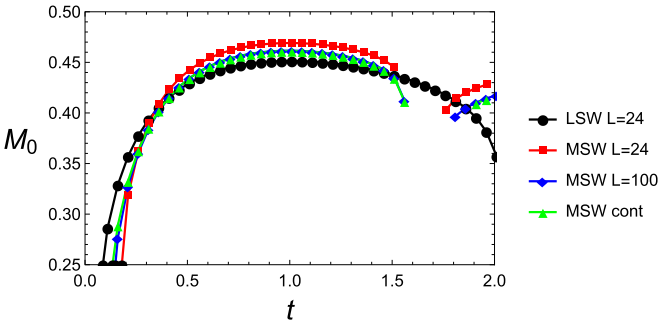

FIG. 5. Occupation of the ground state at zero momentum corresponding to the ordered solution: comparison of results from LSW and from MSW for different sizes of the rhombic-shape lattices with periodic boundary conditions.

have performed without assuming $\nu_{\boldsymbol{k}} \ll 1$ on $L \times L$ rhombic lattices with L up to 10, confirmed this scenario.

Next, we have extended our iterative minimization to larger lattices. We have first studied the half-filling case for $L = 24$ and 100 and for the infinite L limit, obtained by replacing the sum over $\boldsymbol{k}$ with an (numeric) integral over the first Brillouin zone.

B. Phase diagram predicted by spin wave at half-filling

We have first started by studying the half-filling case, $\rho = \frac{\pi}{2}$. Our results are very close to the one of [57] and display the same qualitative behavior (see Fig. 3). In particular, we observe a failure of convergence around $t \sim 0$ and for t between 1.55–1.8. The first region is easily explained: in the limit $t \to 0$, the system reduces to disconnected $1D$-XX chains that can order separately in $1D$-Néel orders with arbitrary relative phases. Thus there is a huge degeneracy in the ground state that should correspond to a gapless spin-liquid phase. The region around $t \sim 1.65$ appears at the interface between two classically ordered phases, the spiral order and a $2D$-Néel order, which appear at lower and higher values of t, respectively. Both phases are well described by the classical order ansatz we used. It is worth noticing that the initial condition and the reflection symmetry of the Hamiltonian around the x axis implies that our solution is respecting such symmetry, i.e., the ordering vector remains parallel to the x axis and the correlation functions respect the relations $F_2 = F(\boldsymbol{\tau}_2) = F(\boldsymbol{\tau}_3) = F_3$, $G_2 = G(\boldsymbol{\tau}_2) = G(\boldsymbol{\tau}_3) = G_3$. This implies that we can work at fixed $Q_y = 0$. For this choice, the $2D$-Néel order corresponds to $Q_x = 2\pi$, while the spiral order corresponds to Q_x smoothly interpolating between 2π and π for decreasing values of the anisotropy t. While at the classical level, the $2D$-Néel order is predicted to be stable for $t \geqslant 2$, the quantum corrections incorporated by MSW approach stabilize it also for lower values of t, as displayed in Fig. 4. Similar results are obtained by exact diagonalization, see Fig. 17(a). By reducing further the values of t the system enters in a nonordered phase signaled by the absence of points from MSW. While in the neighboring regions above and below the nonconvergence window, the occupancy of the zero-momentum states remains large, see Fig. 5, the values of the relative susceptibility ρ_{xx} is small in the vicinity of such window, Fig. 6. Similarly to Ref. [57], we estimate the susceptibility by calculating the Hessian of the energy for fixed correlation functions at the minimum. In order to get an adimensional quantity, we divide by the absolute value of the energy minimum, thus, $\rho_{xx} = \frac{1}{E}\frac{\partial^2 E}{\partial Q_x^2}$, and $\rho_{yy} = \frac{1}{E}\frac{\partial^2 E}{\partial Q_y^2}$. Note that $\rho_{xy} = \frac{1}{E}\frac{\partial^2 E}{\partial Q_x \partial Q_y}$ is identically zero because of the symmetry argument given above. As expected, ρ_{yy} is not signaling any instability for $1.5 \leqslant t \leqslant 2$—the optimal Q_y is identical for the spiral and $2D$-Néel order—while it detects the instability at $t \sim 0$, see Fig. 6. While for all the observables represented in Figs. 4–6 the MSW results deviate considerably from the ones predicted by the LSW, they are quickly converging to a stable behavior for moderate size lattices—for a rhombic shape lattice $L \times L$ the deviation between $L = 24$ and the continuous limit are tiny.

C. Phase diagram predicted by spin wave at generic filling

Then, we have considered lower values of ρ between 0 and $\frac{\pi}{2}$, corresponding to lower densities of Bogoliubov excitations $n = \frac{1}{2}\sin\rho = \frac{1}{2}\sqrt{\nu(1-\nu)}$, where ν is the filling. We have considered the same observables as in the half-filling case. We have found again that the results quickly saturate to a stable

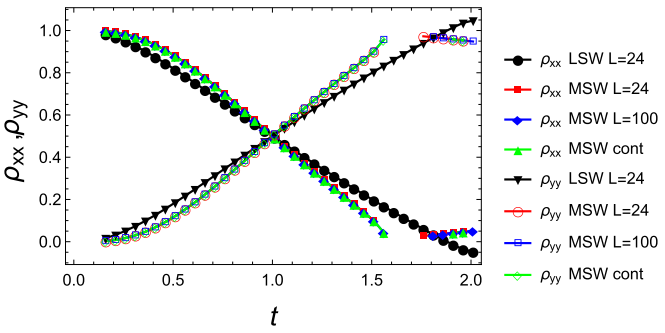

FIG. 6. Values of the rescaled susceptibility ρ_{xx} and ρ_{yy}: comparison of results from LSW and from MSW with different lattice dimensions. Around the nonconvergence window, ρ_{xx} is small, signaling instability of the order. Around the nonconvergence window, ρ_{yy} is large as expected because the y-component of the order vector Q_y is the same for spiral and 2D-Néel order. Instead, ρ_{yy} signals the instability that leads to 1D-Néel order for $t \sim 0$.

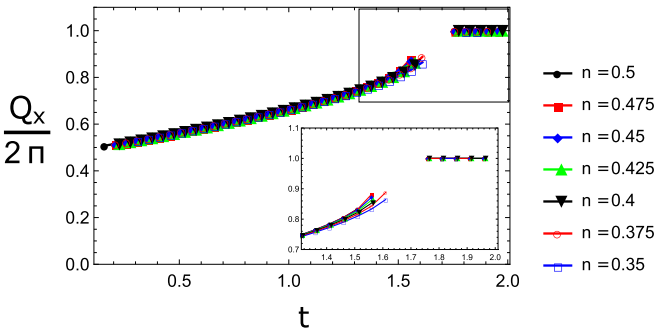

FIG. 7. The value of the optimal Q_x depends in sizable way on the filling only close to the transition to the nonordered region.

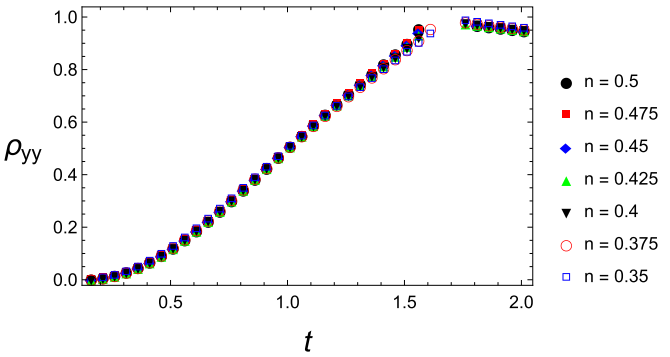

FIG. 9. The value of the rescaled susceptibility ρ_{yy} does not depend considerably on the filling. Indeed, it is sensitive only on the transition at very low t to the 1D behavior, which is unaffected by the filling, while is order 1 around the transition at $t \sim 1.65$.

value for growing size of the lattices. For simplicity, we present here the results $L \times L$ rhombic-shaped lattices with periodic boundary conditions for $L = 100$. First, we notice that the values of the optimal order vector $\boldsymbol{Q}$ remains substantially unchanged with respect to the half-filling case. While by construction $Q_y = 0$, the x-component of the order vector Q_x displays a moderate dependence on n only close to the nonconvergence window, Fig. 7. In fact, the nonconvergence window changes: while it remains centered around $t \sim 1.65$, its extension shrinks smoothly while n decreases. Indications of such behavior can be detected both in the condensate fraction and in the susceptibility. Indeed, the shrinking of the nonconvergence window is well evident in Fig. 8(a) where the occupation of the zero mode M_0 is depicted. As expected M_0 is directly proportional to n, that is to say the condensate fraction $\frac{M_0}{n}$ depicted in Fig. 8(b) is independent of n. This behavior supports the picture that the nature of the ordered phases is unchanged while their stability increase by moving away from half-filling $n = \frac{1}{2}$. Further confirmation comes from the calculation of the relative susceptibilities ρ_{xx} and ρ_{yy}. While ρ_{yy} does not display a strong dependence on n, Fig. 9, ρ_{xx} displays a sizable dependence on n only around the nonconvergence window. In particular, ρ_{xx} weakly increases when n decreases, showing that the ordered phase gets smoothly more stable, Fig. 10. Thus we conclude that by moving out of half-filling the conjectured spin-liquid phase signaled by the nonconvergence window of MSW does not disappear but shrinks rather gently.

V. EXACT DIAGONALIZATION STUDY

In this section, we will study the Hamiltonian (3) by means of exact diagonalization. Therefore we first note that it conserves the z component of total spin, $S_z \equiv \frac{1}{N}\sum_i S_i^z$. This symmetry reflects conservation of particles, and allows to work in Hilbert space blocks with fixed spin polarization. Using this symmetry, we are able to exactly diagonalize systems of up to 24 sites. We mostly consider open boundary conditions (i.e. hard walls), which not only mimicks best the trapped scenario we have in mind, but also allows for arbitrary ordering vectors. We have studied different geometries, in particular the highly symmetric arrangement depicted in Fig. 2(a), but also rhombic arrangements shown in Fig. 2(b), which can systematically be scaled from 12 to 24 by adding rows of four spins.

As in the spin-wave analysis, we will first consider the system within a local density approximation, assuming homogeneity within shells of different S_z. Our exact diagonalization study is expected to capture the system behavior in the center of the trap, and we set $V_i = 0$. Afterwards, we study effects of the trapping potential on small scales, diagonalizing Eq. (3) at finite V_i. The exact diagonalization study presented here covers the case at half-filling ($S_z = 0$) known from Refs. [51,57], with a possible quantum spin liquid for $t \approx 0.5$ and $t \approx 1.5$. We extend this study to other polarization sectors, which become relevant if the trap leads to an increased density in the center.

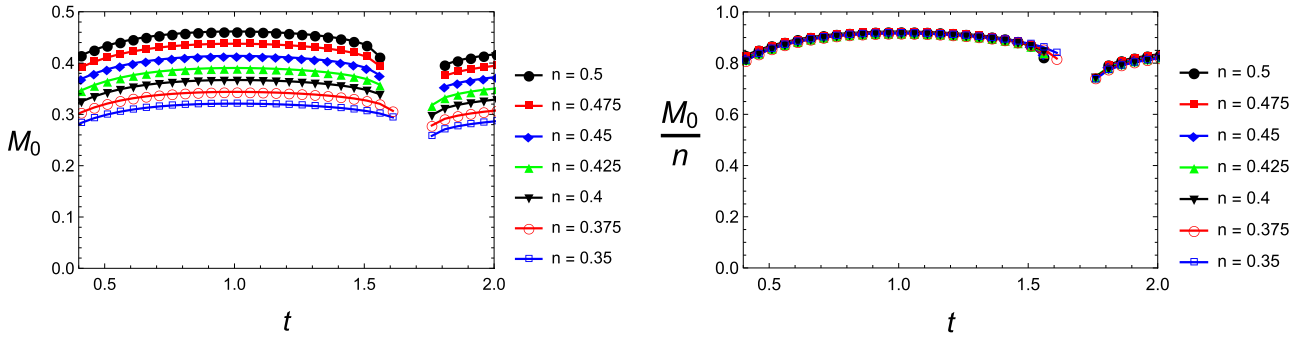

FIG. 8. (a) Occupation of the state at zero momentum for different filling: the nonordered region shrinks smoothly with the filling. (b) The condensate fraction is independent of the filling in the ordered regions.

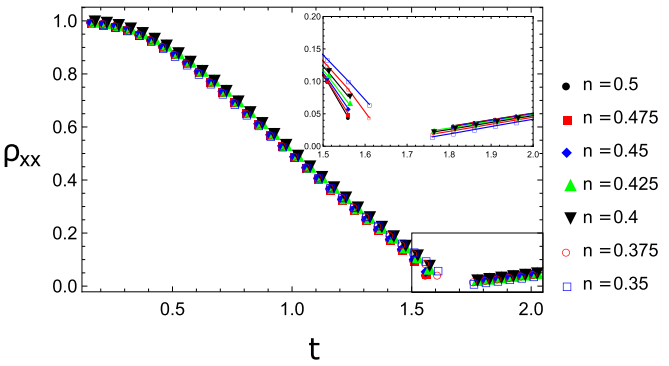

FIG. 10. The value of the rescaled susceptibility ρ_{xx} depends sizably on the filling only close to the transition to the nonordered region. A slighter increase of ρ_{xx} at lower n translates in an increased stability of the ordered phases.

A. Homogeneous system ($V_i = 0$)

As an experimentally accessible quantity which allows to chararacterize the order of the system, we have calculated the magnetic structure factor $S(\mathbf{Q})$:

$$S(\mathbf{Q}) = \frac{2}{N}\sum_{i,j}\exp[i\mathbf{Q}\cdot(\mathbf{r}_i - \mathbf{r}_j)]\langle S_i^+ S_j^- + \text{H.c.}\rangle. \quad (35)$$

Here, $\langle\cdot\rangle$ denotes the quantum average of the ground state. This quantity is the Fourier transform of the total magnetization in the S_x-S_y plane, and therefore magnetic order is signalled by a pronounced peak. The momentum space position $\mathbf{Q}$ of the peak further characterizes the spatial ordering of the magnetization. Based on $S(\mathbf{Q})$, we define magnetization M as a relevant order parameter

$$M = \sqrt{S(\mathbf{Q})/N}. \quad (36)$$

At all fillings and for all anisotropies, M has a global maximum for $Q_y = 0$, with the corresponding Q_x varying between π and 2π as a function of t, see Fig. 11(a). The two limiting values $Q_x = \pi$ and $Q_x = 2\pi$, obtained for $t = 0$ and $t \gtrsim 1.6$, correspond to an intrachain Néel order, and to a square-lattice Néel order, respectively. Remarkably, for most values of t, the peak momentum Q_x hardly depends on the spin polarization, with the exception of a small region around $t \approx 1.5$, where $\mathrm{d}Q_x/\mathrm{d}t$ tends to infinity. This means that in a trapped system, composed of subsystems with different S_z, each subsystem would produce the same signal when the magnetic structure factor is measured. As a result, one would measure same peak as in the homogeneous system, except for a possible broadening of the peak near $t \approx 1.5$.

In Fig. 11(b), we show the order parameter M for different polarization sectors. In comparison to Q_x, there are some quantitative dependencies on the polarization, but qualitatively, the curves still share many qualitative properties: with few exceptions, M always increases with t, but typically regions of rapid increase are followed by rather flat regimes. A strong tendency for rapid increase occurs at $t \approx 0.6$ and for $t \gtrsim\approx 1.5$. For most S_z, a small region in which M decreases with t, is found within a small region at $t \lesssim 1.5$. Note that for $S_z = 0$ this dip is absent, but instead the curve exhibits a kink at $t \approx 1.5$, with $dM/dt = 0$. These dips/kinks might be interpreted as a signal for quantum spin liquid behavior, as they indicate the loss of the magnetic order.

We also note that, based on a PEPS study in Ref. [57] in a 20×20 lattice, another spin liquid regime is expected around $t \approx 0.5$, that is, just before the first rapid increase of M. This expectation is based on a dip in $M(t)$ near $t \approx 0.5$, which is found in larger systems. Within our study on the $N = 24$ lattice, though, the magnetic order parameter does not signal spin liquid behavior in this region.

Additional information regarding the presence or absence of magnetic order can be obtained from the dependence of the order parameter on the number of spins N. For such scaling analysis, we perform exact diagonalization at half-filling on a graph as shown in Fig. 2(b). The results are shown in Fig. 12. Before analyzing the size dependecies in Fig. 12, we may focus on the curve for $N = 24$ and compare it with the corresponding in Fig. 11(b). As finite-size effects should strongly depend on the geometry of the system, such comparison may help to distinguish bulk behavior from edge effects. We find that, for $t \gtrsim 1$, the magnetization M exhibits very similar behavior in both geometries, in particular regarding the kind at the $t \approx 1.5$ followed by a sharp increase. For larger values, $t \gtrsim 1.6$, the

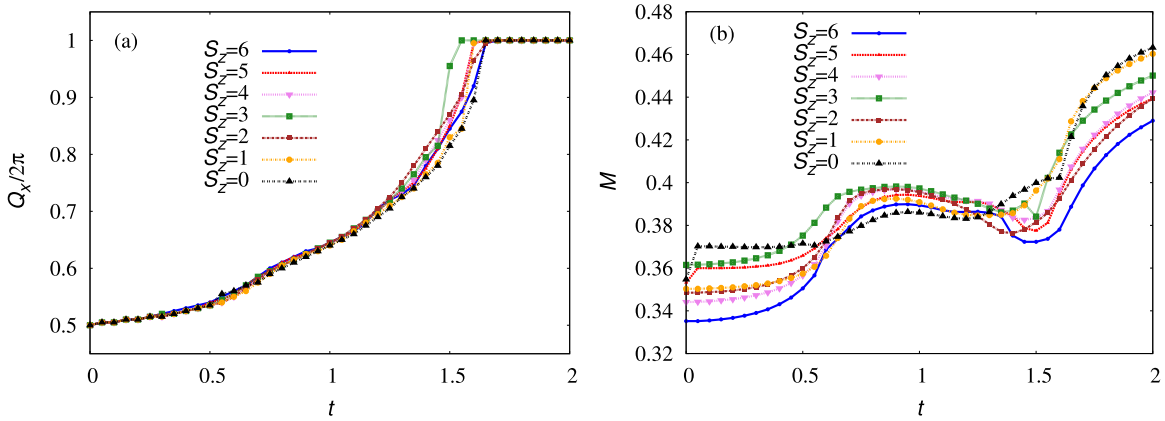

FIG. 11. In different polarization sectors S_z, we evaluate (a) the position of peak of structure factor $S(\mathbf{Q})$ as a function of anisotropy t, and (b) the magnetic order parameter M, as defined in Eq. (36) from the peak value of $S(\mathbf{Q})$. We consider a homogeneous system ($B_i = 0$) with $N = 24$ spin, arranged in the hexagonal geometry shown in Fig. 2(a).

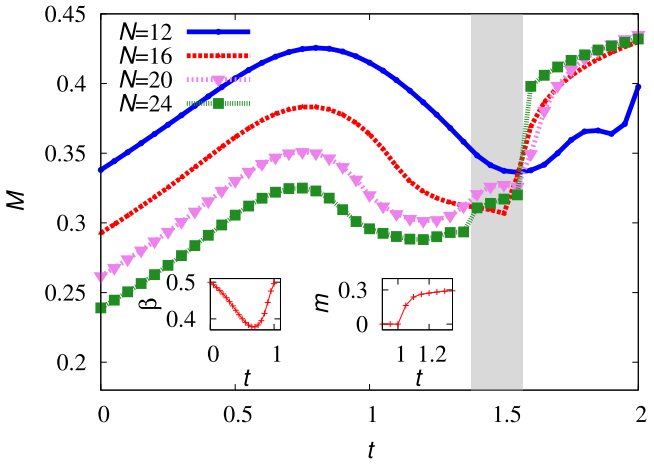

FIG. 12. Magnetic order parameter M as a function of lattice anisotropy t, for different number of spins N in the rhombic arrangement depicted in Fig. 2(b). The inlays show the results of extrapolating the data to $1/N \to 0$ using the fit function $f(N) = \alpha N^{-\beta} + m$, with $m > 0$. For $t \leqslant 1$, we get $m = 0$ and an exponent $\beta \approx 0.5$, as shown in the left inlay. For $1 < t < 1.35$, the data extrapolate to finite values of m, see right inlay. In the shaded region, $1.35 < t < 1.56$, the system is disordered in the sense that the data do not behave monotonically with N. For larger t, the data converges quickly to a size-independent value which approaches the value $M_0 = 0.437$ for a Neel-ordered square lattice (cf. Ref. [70]).

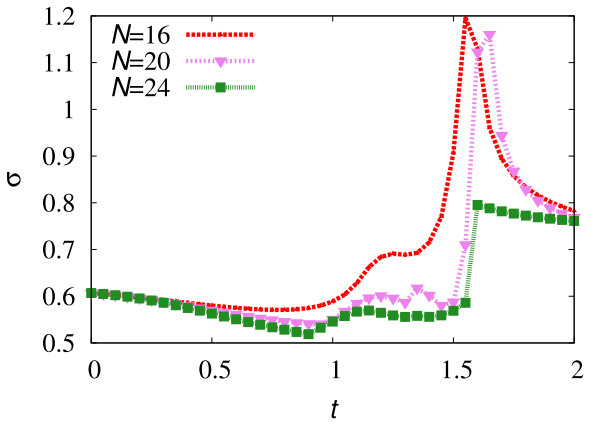

FIG. 13. Width σ of the structure factor peak as a function of t, for a rhombic arrangement of the spins. A broadening of the peak near $t \approx 1.5$ is observed for all system sizes, but is most pronounced for smaller systems ($N = 16$ and $N = 20$).

magnetization saturates. As discussed before, the kink could be the sign of a spin liquid phase, and strikingly, this feature does not depend on the geometry of the system. Also the flat regime for large t is barely affected by the geometry, and is interpreted the Neel ordered phase in a square lattice (equivalent to the rhombic lattice structure for $t \to \infty$). A striking observation which backs this interpretation is the value of M obtained at large t in the rhombic geometry: it approaches precisely the value $M = 0.437$ expected for a square lattice [70].

Next, we will analyze size dependencies, which play an important role for $t \lesssim 1.6$. The whole region can be divided into two regimes; while for $t < 1.35$ the order parameter M behaves monotically with N, this is not the case for $1.35 < t < 1.6$. We may interpret this nonmonotonic behavior as a signal for the lack of magnetic order. The finite value of M can then be seen a random effect due to the limited system size. Such scenario agrees with a spin liquid phase, however, we cannot rule out complicated orderings which are, in a nonmonotonic way, sensitive to the finite size of the system.

For $t < 1.35$, the monotonic behavior of $M(N)$ allows for a quantitative scaling analysis. Using the fit function $f(N) = \alpha N^{-\beta} + m$ with real fit parameters α, β, and m, we obtain the unphysical result $m < 0$ for $t < 1$. We conclude that in this regime, no magnetization survives in the thermodynamic limit, and set $m = 0$. We then find an exponent $\beta \approx 0.5$ as shown in the left inlay of Fig. 12. The exponent $1/2$ agrees with exponential decay of correlations, $S(\mathbf{Q})/N \sim \int_0^{\sqrt{N}} dr\, r \exp(-r/\xi) \sim 1/N$, with ξ denoting the correlation length. For $t > 1$, we obtain finite positive values of m, as shown in the right inlay of of Fig. 12, indicating that the system remains magnetized in the thermodynamic limit.

Another relevant quantity which can be obtained from the magnetic structure factor is the width of the peak. To account for the difference in height, we normalize $S(\mathbf{Q})$ with $S(\mathbf{Q}_{\text{peak}})$. For simplicity, let us assume that the peak of the structure factor has a Gaussian shape. The width of the peak is then given by the standard deviation σ, which can be obtained from the second derivative at the peak. Along the Q_x direction, we have

$$\sigma = \left(\frac{1}{S(\mathbf{Q}_{\text{peak}})} \left[\frac{\mathrm{d}^2}{\mathrm{d}Q_x^2} S(Q_x, Q_y) \right]_{\mathbf{Q}=\mathbf{Q}_{\text{peak}}} \right)^{-1/2}. \tag{37}$$

We have evaluated this quantity for rhombic systems as shown in Fig. 13. The most remarkable feature is the rapid increase of σ near $t = 1.5$, i.e., a significant broadening of the peaks for $N = 16$ and $N = 20$, indicating a loss of magnetic order. For $N = 24$, however, the data shows a slightly different behavior: Although a global maximum is still exhibited at $t = 1.5$, the extremum is less pronounced than in the other cases. Interestingly, no size dependence of σ occurs in the two limits $t \to 0$ and $t \to \infty$.

To shed more light onto the regime $1.35 < t < 1.6$, we will now consider the possibility of nonmagnetized order. A clear candidate for a nonmagnetized but ordered phase is the so-called valence-bond crystal (VBC). In this phase, nearest-neighbor spins are dimerized, and the dimers form a regular pattern. Since $t > 1$, dimerization should preferably occur along the two diagonal directions (i.e., those with strength t_2). We assume the simplest case, in which (spontaneously or due to the finite size) one of these two direction is chosen by all dimers. In our case, the rhombic shape in Fig. 2(b) enhances dimerization along the links pointing to the upper neighbor on the right. Denoting each spin with a single index i, possible dimers might be formed between spin i and spin $i + R$, where R is the number of spins in a row, see also Fig. 3 for an illustration of this notation. Correlations between these dimers are measured by the following structure factor:

$$S_D(\mathbf{Q}) = \frac{1}{N} \sum_{i \neq j} \mathrm{e}^{i\mathbf{Q}\cdot(\mathbf{r}_i - \mathbf{r}_j)} [\langle (\mathbf{S}_i \cdot \mathbf{S}_{i+R})(\mathbf{S}_j \cdot \mathbf{S}_{j+R}) \rangle - \langle \mathbf{S}_i \cdot \mathbf{S}_{i+R} \rangle \langle \mathbf{S}_j \cdot \mathbf{S}_{j+R} \rangle]. \tag{38}$$

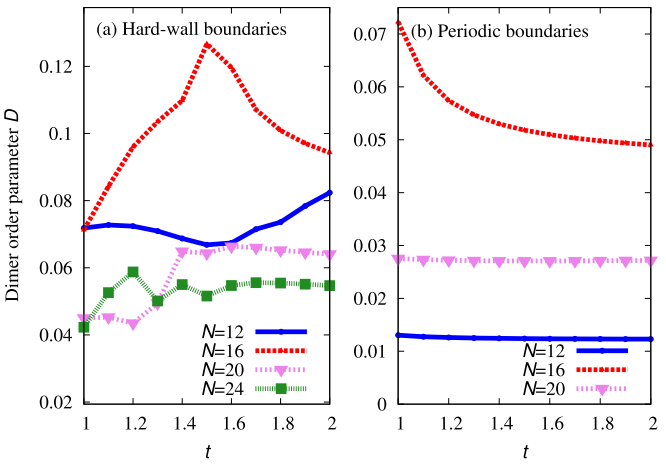

FIG. 14. Dimer order parameter D as a function of lattice anisotropy t, for different number of spins N in the rhombic arrangement depicted in Fig. 2(b). We consider both open boundaries (a), and periodic boundaries (b). Most curves are relatively flat at a constantly small value of D, suggesting that there is no VBC-ordered regime. The peak around $t \approx 1.5$ for $N = 16$ in an open geometry seems to be a finite-size effect, as this effect is not present for other values of N. It may be due to the limited number of perfect dimer coverings possible in small lattices.

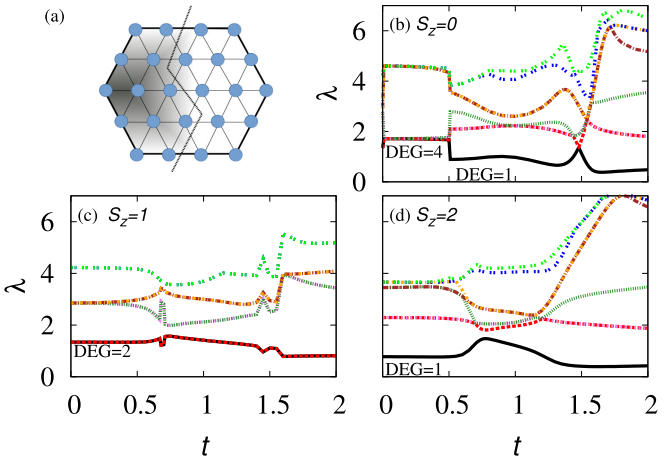

FIG. 15. Entanglement spectrum (eight lowest values) for different spin polarizations (b)–(d), obtained in a $N = 24$ hexagonally shaped lattice with the cut shown in (a). DEG denotes the number of (quasi-)degenerate levels in the ground state.

Again we define an order parameter D by considering the peak value of S_D:

$$D = S_D(\mathbf{Q}_{\text{peak}})/N. \tag{39}$$

Both the vector $\mathbf{Q}_{\text{peak}}$ as well as the behavior of D as a function of t depend sensibly on the size of the system, and on the geometry, see Fig. 14 showing results for a rhombic system with open or periodic boundary conditions (i.e., hard walls or period). We conclude that the small finite values of D are random finite-size effects, and the flatness of most curves suggest that at no value of t VBC order is established. A single exception occurs for $N = 16$ with open boundary. However, as other sizes (in particular $N = 24$ with even number of rows) does not show any sign of a similar peak, we shall not interpret this as a sign for VBC order. Note that, due to the boundary conditions, there is only a single way of perfectly covering the whole lattice with nearest-neighbor dimers (for even number of rows). Alternative coverings leave few spins without dimer, with an energy cost which plays the biggest role in small systems. This might cause enhanced VBC order in very small systems, while does not give rise to any effects in systems with larger bulk.

The order parameters M and D discussed so far directly measure certain types of order, or, by excluding the corresponding order, they can give hints for spin liquid behavior. However, they cannot positively detect a spin liquid and its topological order. It is subject to current research which quantities may serve as topological order parameters, and the entanglement spectrum has been shown to be a promising candidate. In fact, Ref. [71] demonstrates that for the Haldane phase of a $S = 1$ chain, the entanglement spectrum is doubly degenerate due to a hidden symmetry. The presence of magnetic order can be detected by the entanglement spectrum through tower-of-states structures, which have been shown to be in correspondence with the low energy spectrum in a DMRG study of the J_1-J_2 Heisenberg model on the triangular and the kagome lattice [72]. Here, we restrict our discussion in the following to degeneracies of the entanglement spectrum, which does not require the determination of the quantum numbers of each entanglement eigenvector. Although degeneracies of the entanglement spectrum are not a robust criterion for topological order, it will be interesting to see whether degeneracies occur in those regimes which we have identified above as possible spin liquid phases.

The entanglement spectrum is obtained from the eigenvalues of the reduced density matrix $\rho_{\text{L}} \equiv \text{Tr}_{\text{R}}|\Psi\rangle\langle\Psi|$. Here, Tr_{R} denotes a trace over half spins, localized on the right side of the lattice. The entanglement spectrum is then defined as $\lambda_i = -\ln \rho_i$, where ρ_i denote the eigenvalues of ρ_{L}. In Figs. 15 and 16, we plot the eight lowest values of the entanglement spectrum as a function of the anisotropy t in a homogeneous system of 24 spins. In Fig. 15, we consider a hexagonal spin arrangement and study the dependence of the entanglement spectrum on the spin polarization S_z. In Fig. 16, we focus on a rhombic system and consider different ways of cutting it into two subsystems. While in general the entanglement eigenvalues are not universal, certain properties of the entanglement spectrum, like degeneracies of levels, may reflect certain symmetries, and should thus be independent from the cut.

Comparing the entanglement spectra at different spin polarizations, the most interesting behavior is exhibited at $S_z = 0$. Here, the number of degeneracies strongly depends on the parameter t. In contrast, for odd polarization sectors (as illustrated in Fig. 15 for $S_z = 1$), each level is doubly degenerate for any t. For $S_z = 2$, the ground-state level remains unique for all t, and only higher levels exhibit some t-dependent degeneracies. For $S_z = 0$, in Fig. 15, the most notable feature is a degenerate regime for $t \leqslant 0.5$ with an exact double degeneracy of each level. Doubly degenerate levels give further rise to quasidegenerate manifolds: the ground-state level is has a fourfold quasidegeneracy, followed

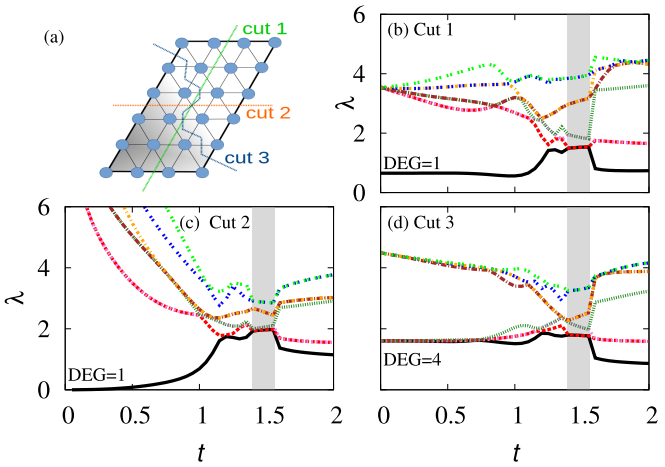

FIG. 16. On a rhombic shaped lattice ($N = 24$ sites), we evaluate the entanglement spectrum for different cuts shown in (a). The eight lowest values of each entanglement spectrum are shown in (b)–(d). The spin polarization is fixed to $S_z = 0$. DEG denotes the number of (quasi)degenerate levels in the ground state. The grey area around $t \approx 1.4$, mark the regime where each level exhibits a twofold degeneracy.

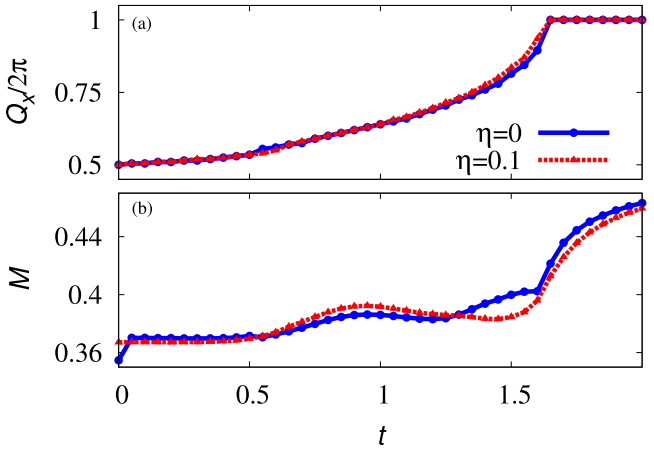

FIG. 17. (a) Position Q_x of peak of structure factor $S(\mathbf{Q})$ as a function of anisotropy t at $S_z = 0$ in a homogeneous system and for $\eta = 0.1$. (b) Order parameter M as defined in Eq. (36).

by quasiflat manifolds containing 24, 76, and 176 levels. Note that the regime in which the entanglement spectrum exhibits degeneracies coincides with the regime in which a spin liquid phase was suspected by Ref. [57]. In contrast, for $0.5 < t < 1.48$, the entanglement spectrum exhibits a unique ground state level, with double degeneracies present in the excited levels. Strikingly, at $t = 1.48$, a level crossing leads to double degeneracy not only of the ground state, but crossings also occur between other levels at the same (or a similar) value of t. This leads to the scenario that, around $t \approx 1.48$, levels are pairwise quasidegenerate (or degenerate). Interestingly, this region coincides with the regime where, based on our previous analysis of order parameters M and D, we expect to have a spin liquid.

In Fig. 16, we focus on the fully unpolarized system ($S_z = 0$), and investigate the dependence of the entanglement spectrum for different cuts through a rhombic system, as illustrated in Fig. 16(a). The most natural cuts are the ones parallel to one side of the rhombus. Clearly, in one of these two cases, the entanglement between the subsystems fully vanishes in the highly anisotropic regime $t \to 0$, because different rows do not interact. With our choice of having an even number of spins per row, also the other cut produces low entanglement, since in each row the two spins on the left and right sides produce dimers, with little entanglement between the second and the third spin. Accordingly, these two cuts do not reproduce the exact twofold degeneracy which we had found in the hexagonally shaped lattice at small t. However, the unsymmetric cut shown in Fig. 16 again leads to a fourfold quasidegeneracy of the ground state up to values of t as large as 0.8.

A clearer picture arises around $t \approx 1.4$. Independent of the cut, we find a sizable interval $1.38 \lesssim t \lesssim 1.55$, in which all levels are exactly twofold degenrate. This finding gives a much stronger support for a spin liquid phase than the quasidegeneracies due to level crossings, which we had found for $t \approx 1.48$ in the hexagonal system. We also stress that the lowest entanglement eigenvalue barely depends on neither the cut nor the system geometry, suggesting that the system forms a uniform liquid in this region of t.

B. Inhomogeneous system ($V_i \neq 0$)

In the previous paragraph, we have shown that the system, to some extent, behaves similarly in different polarization sectors upon tuning the anisotropy t. This allows one to argue that the same behavior should persist in a shallow trap, where the system is approximated by homogeneous subsystems of different polarizations. In the present paragraph, we go a step further, and analyze the effect of a trap on short scales by diagonalizing Hamiltonian (3) for $V_i = \frac{m}{2}\omega^2 \mathbf{r}_i^2 = \eta \mathbf{r}_i^2$, with $\eta = 0.1$ (in units t_1/a^2) for typical trapping frequencies of 40 Hz. We will focus on the $S_z = 0$ sector, corresponding to half-filling.

On the small lattice studied here, the inhomogeneities introduced by the trap, are rather weak: for the isotropic system, $t = 1$, we find an average population of 0.46 atoms on the 14 sites at the edge of the lattice, while the remaining 10 sites have an average population of 0.56 atoms. Accordingly, also the structure factor is barely modified: as shown in Figure 17(a), the peak position Q_x is practically indistinguishable for the two cases $\eta = 0$ and $\eta = 0.1$. Also the magnetic order parameter M, shown in Fig. 17(b), exhibits a similar shape, though slightly smoothened near $t = 1.5$. Also the entanglement spectrum, plotted in Fig. 18, shares important qualitative features with the one of the homogeneous system shown in Fig. 15(a): for small values of t the ground-state level has a perfect twofold degeneracy, and a fourfold quasidegeneracy. Again, the lifting of the degeneracy occurs abruptly near $t \approx 0.5$, although the precise value of the anisotropy is slightly increased by the trap. However, the level crossing observed in the homogeneous case around $t \approx 1.5$ does not take place in the trapped scenario. Whether this result questions the presence of a spin liquid phase in the trapped system, or whether degeneracies in the entanglement spectrum provide a relevant criterion for spin liquid behavior, cannot be decided

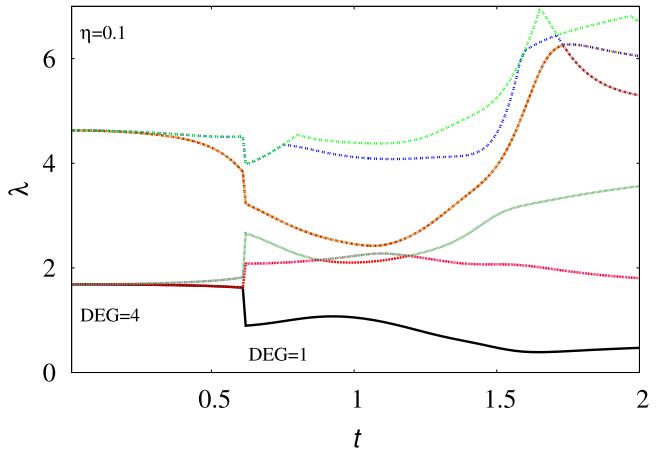

FIG. 18. Entanglement spectrum (eight lowest values) at $S_z = 0$ in a trapped system at $\eta = 0.1$. D denotes the number of degenerate levels in the ground state.

here. Here, we find it interesting to notice that, while the behavior of the magnetic order parameter is hardly affected by the trap, the entanglement spectrum changes considerably.

To shed more light onto the role of the trap, we finally turn our attention to the excitation spectra. For selected t, we compare the spectra of the trapped and the homogeneous system in different polarization sectors in Figs. 19(a)–19(d). For the spectra of the homogeneous system, a tower-of-state feature [73,74] has been noticed in Ref. [57]. In all polarization sectors, around $t = 1$ and $t = 2$, a small number of states at low energy is separated from states at higher energy by a large gap. This low-energy manifold is the basis from which Néel or spiral order can arise. In the thermodynamic limit, low-energy states at different S_z approach the same energy, and U(1) symmetry can spontaneously be broken. In contrast to this, relatively homogeneous level spacings are observed around $t \approx 0.6$ and $t \approx 1.4$ in *all* polarization sectors. Accordingly, a tower-of-state argument cannot be applied to those spectra, giving some evidence that no ordered phase will occur in these regions.

To quantify this different behavior, we shall look at the gap in each polarization sector. However, quasidegeneracies make it difficult or impossible to distinguish between levels which still should be considered ground states and excited states. For this reason, we will simply consider the largest level spacing $s_{\max}(S_z)$ within the ten lowest states. The "tower of states" argument is applicable, if $s_{\max}$ is large in many or most polarization sectors. This would result in a large average value $\langle s_{\max}\rangle$, where the average is taken with respect to different spin polarizations. We further normalize this value by dividing by full spacing between the ten levels, such that $s_{\max}$ is maximal (=1) if the ten states are divided into two degenrate manifolds, while it is minimal (=0.1) if the levels are spaced homogeneously and the spectrum lacks a clear separation between low- and high-energy manifolds. Accordingly, a breakdown of the tower-of-state argument is indicated by minima of $s_{\max}$. This average is shown in Fig. 19(e), for both a trapped and a homogeneous system. In both cases, it exhibits one pronounced minimum near $t \approx 0.6$. A second, less pronounced minimum is found around $t \approx 1.65$, which becomes further washed out in the presence of a trap.

VI. CONCLUSIONS AND OUTLOOK

In this paper we have studied the fate of QSL phases in realistic experimental conditions, namely, in presence of an harmonic confinement. The modified spin wave theory, which was previously formulated for bosons in a triangular lattice at half-filling, has been re-derived for arbitrary filling factors. With this generalization, it can be used to capture, within a local density approximation, the physics of inhomogeneous systems. We have shown that the prediction of spin liquid behavior for an anisotropy $t \approx 1.65$ does not depend much on the filling factor, and should therefore survive in a trapped gas. This expectation has been backed by results from exact diagonalization in lattices of different sizes and geometries, up to 24 sites. Our exact diagonalization analysis has also ruled out the presence of an ordered nonmagnetic phases like VBC that could explain the breaking of magnetic order in alternative

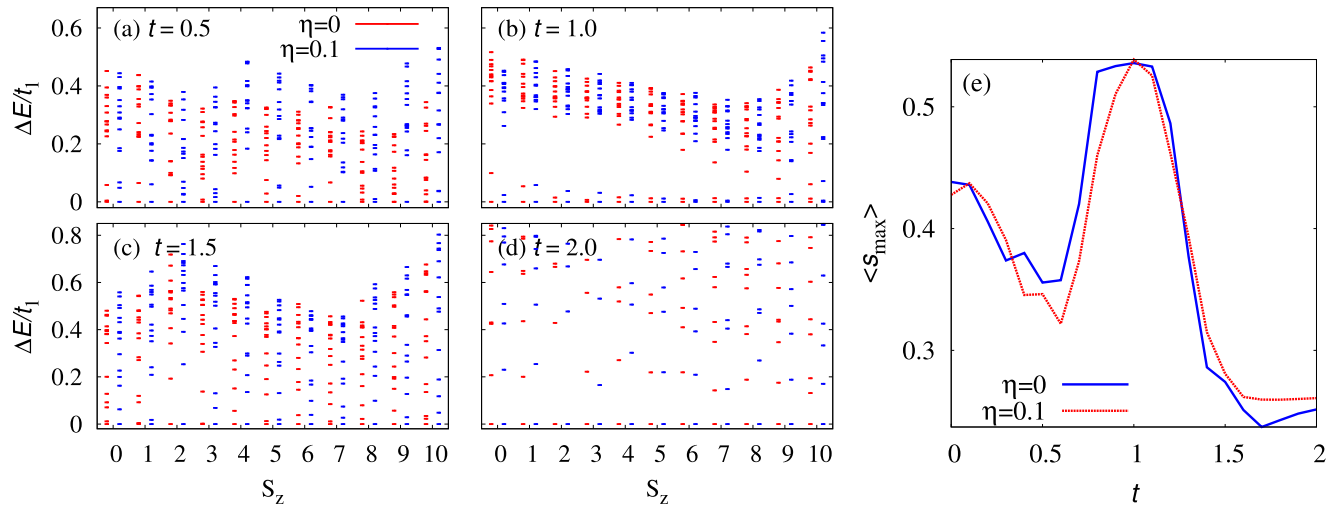

FIG. 19. (a)–(d) Energy vs spin polarization at different t's for $S_z = 0$ in a trapped system for $\eta = 0.1$ and $\eta = 0$. (e) Largest level spacing $s_{\max}$ amongst ten lowest levels averaged over all polarization sectors, for a trapped system at $\eta = 0.1$ and for $\eta = 0$.

to a QSL phase. These results support the existence of another QSL region at lower anisotropy, $t \approx 0.6$, which is not detected by MSW. Such discrepancy is not surprising. It is reasonable to expect that the MSW is able to detect a QSL phase only between two classical ordered phases—the QSL phase at $t \approx 1.65$ appears between spiral and $2D$-Néel phases–while it is blind to transitions that are purely quantum. One may wonder that this happens only because the optimization is done starting by the classical solution. In fact unbiased direct searches of global minima provided the same or more energetic metastable solutions. Apparently, the optimal solution of the MSW is always a deformation of the classical one: perhaps, this is not so surprising because the spin wave approach is an expansion in $\frac{n}{2S}$ and the terms in $(\frac{n}{2S})^2$ included in the MSW are corrections to the terms considered in the LSW. The exact diagonalization approach have allowed us also to go beyond the local density approximation, and to study inhomogeneities on small scales. On this level, we have found no essential effect due to the trap for realistic choices of the trapping frequency. While the finite-size corrections are certainly expected to affect the exact diagonalization results, they should not exceed the 10%–20%. As the observables computed are global one would argue that the QSL behavior extends at least to entire lattice (of 24 spins) considered. The finite-size scale analysis we have performed in the homogeneous case further supports this picture. While final-size effects are not directly visible in the MSW because we have used periodic boundary conditions, they enter by determining the quality of local density approximation. Until the trap is not steep, and at the center is never so, the MSW suggests that, by taking optimal value of $t \approx 1.65$ at the center of the QSL region, the QSL phase should be visible even if the filling is changing considerably. Suppose, for instance, that the trap is tuned to have an occupation of around 3.7 atoms per site at the center, that to say 20% above the half-filling condition. Then, we could conclude that if we reach an occupation of 3.3 atoms per site –20% below half-filling—at 10 lattice sites or more from the center, at the same time, we are within validity of local-density approximation in the QSL phase as predicted by MSW theory, and we limit the corrections due to the finite size as they are expected to go down as the inverse of the diameter of the region considered. Our study therefore provides strong hints for a robust QSL phase of bosons in anisotropic triangular lattices with antiferromagnetic tunnelings, which is not affected by weak trapping potentials as used in experiments.

The robustness of the QSL phase in presence of a weak harmonic confinement allow for the experimental investigation of these exotic quantum phases. The realization of the XX Hamiltonian for bosons in the strongly correlated regime relies on the periodic driving of the triangular optical lattice, which allows inverting the sign of the tunneling matrix elements as well as controlling their amplitude. The ability to tune the tunneling amplitude independently from the on-site interaction allows reaching strongly correlated phases where $U \gg |J_{\rm eff}|$ without increasing the lattice depth. Indeed, as the effective tunneling $J_{\rm eff}$ follows a zeroth-order Bessel function as the shaking amplitude is increased, the system shall first enter a Mott-insulating phase before reaching the anti-ferromagnetic side of the phase diagram and thus the quantum spin liquid phase. Such a trajectory has allowed for a reversible crossing of the superfluid to Mott-insulator phase transition in a driven cubic lattice [54]. One limiting factor, however, are multiphoton resonances to higher lying Bloch bands, which critically reduce the coherence of the bosonic gas [75]. These resonances occur when a multiple of the shaking frequency matches the gap between the renormalized bands. Therefore an optimized scheme for crossing the quantum phase transition while avoiding such resonances has to be developed.

ACKNOWLEDGMENTS

We acknowledge financial support from the EU grants EQuaM (Seventh Framework Programme-ICT-2013 No. 323714), OSYRIS (European Research Council-2013-AdG No. 339106), SIQS (Seventh Framework Programme-ICT-2011-9 No. 600645), QUIC (Horizon 2020-FETPROACT-2014 No. 641122), Spanish Ministerio de Economía y Competitividad grants (Severo Ochoa SEV-2015-0522 and FOQUS FIS2013-46768-P), Generalitat de Catalunya (2014 SGR 874), and Fundación Cellex.

[1] L. Balents, Nature (London) **464**, 199 (2010).
[2] P. W. Anderson, Mater. Res. Bull. **8**, 153 (1973).
[3] P. W. Anderson, Science **235**, 1196 (1987).
[4] S. A. Kivelson, D. S. Rokhsar, and J. P. Sethna, Phys. Rev. B **35**, 8865 (1987).
[5] V. Kalmeyer and R. B. Laughlin, Phys. Rev. Lett. **59**, 2095 (1987).
[6] X.-G. Wen, F. Wilczek, and A. Zee, Phys. Rev. B **39**, 11413 (1989).
[7] G. Misguich and C. Lhuillier, in *Frustrated Spin Systems*, edited by H.T. Diep (World Scientific, Singapore, 2003).
[8] C. Lhuillier, arXiv:cond-mat/0502464.
[9] F. Alet, A. M. Walczak, and M. P. A. Fisher, Physica A **369**, 122 (2006).
[10] C. Waldtmann, H.-U. Everts, B. Bernu, C. Lhuillier, P. Sindzingre, P. Lecheminant, and L. Pierre, Eur. Phys. J. B **2**, 501 (1998).
[11] N. Read and S. Sachdev, Phys. Rev. Lett. **66**, 1773 (1991).
[12] X.-G. Wen, Phys. Rev. B **44**, 2664 (1991).
[13] X.-G. Wen, *Quantum Field Theory of Many-body Systems* (Oxford University Press, Oxford, 2004).
[14] A. Y. Kitaev, Ann. Phys. (NY) **303**, 2 (2003).
[15] R. Moessner and S. L. Sondhi, Phys. Rev. Lett. **86**, 1881 (2001).
[16] R. Moessner and S. L. Sondhi, Prog. Theor. Phys. **145**, 37 (2002).
[17] O. I. Motrunich, Phys. Rev. B **72**, 045105 (2005).
[18] Y. Shimizu, K. Miyagawa, K. Kanoda, M. Maesato, and G. Saito, Phys. Rev. Lett. **91**, 107001 (2003).
[19] T.-K. Ng and P. A. Lee, Phys. Rev. Lett. **99**, 156402 (2007).
[20] F. L. Pratt, P. J. Baker, S. J. Blundell, T. Lancaster, S. Ohira-Kawamura, C. Baines, Y. Shimizu, K. Kanoda, I. Watanabe, and G. Saito, Nature (London) **471**, 612 (2011).
[21] T.-H. Han, J. S. Helton, S. Chu, D. G. Nocera, J. A. Rodriguez-Rivera, C. Broholm, and Y. S. Lee, Nature (London) **492**, 406 (2012).

[22] M. Fu, T. Imai, T.-H. Han, and Y. S. Lee, Science **350**, 655 (2015).

[23] M. Amusia, K. Popov, V. Shaginyan, and V. Stephanovich, *Theory of Heavy-Fermion Compounds - Theory of Strongly Correlated Fermi-Systems* (Springer-Verlag, Berlin, Heidelberg, 2014).

[24] S. Yan, D. A. Huse, and S. R. White, Science **332**, 1173 (2011).

[25] S. Depenbrock, I. P. McCulloch, and U. Schollwöck, Phys. Rev. Lett. **109**, 067201 (2012).

[26] M. Levin and X.-G. Wen, Phys. Rev. Lett. **96**, 110405 (2006).

[27] A. Kitaev and J. Preskill, Phys. Rev. Lett. **96**, 110404 (2006).

[28] S. Furukawa and G. Misguich, Phys. Rev. B **75**, 214407 (2007).

[29] S. V. Isakov, M. B. Hastings, and R. G. Melko, Nat. Phys. **7**, 772 (2011).

[30] Y. Zhang, T. Grover, and A. Vishwanath, Phys. Rev. Lett. **107**, 067202 (2011).

[31] H.-C. Jiang, Z. Wang, and L. Balents, Nature Phys. **8**, 902 (2012).

[32] Y. Zhang, T. Grover, and A. Vishwanath, Phys. Rev. B **84**, 075128 (2011).

[33] Y. Zhang, T. Grover, and A. Vishwanath, New J. Phys. **15**, 025002 (2013).

[34] M. Punk, D. Chowdhury, and S. Sachdev, Nat. Phys. **10**, 289 (2014).

[35] A. Wietek, A. Sterdyniak, and A. M. Läuchli, Phys. Rev. B **92**, 125122 (2015).

[36] K. Kumar, K. Sun, and E. Fradkin, Phys. Rev. B **92**, 094433 (2015).

[37] F. Kolley, S. Depenbrock, I. P. McCulloch, U. Schollwöck, and V. Alba, Phys. Rev. B **91**, 104418 (2015).

[38] H.-C. Jiang, H. Yao, and L. Balents, Phys. Rev. B **86**, 024424 (2012).

[39] S.-S. Gong, W. Zhu, and D. Sheng, Sci. Rep. **4**, 6317 (2014).

[40] S.-S. Gong, W. Zhu, L. Balents, and D. N. Sheng, Phys. Rev. B **91**, 075112 (2015).

[41] A. Kitaev, Ann. Phys. **321**, 2 (2006), January Special Issue.

[42] I. Kimchi and A. Vishwanath, Phys. Rev. B **89**, 014414 (2014).

[43] K. Li, S.-L. Yu, and J.-X. Li, New J. Phys. **17**, 043032 (2015).

[44] I. Rousochatzakis, U. K. Rössler, J. van den Brink, and M. Daghofer, Phys. Rev. B **93**, 104417 (2016).

[45] M. Lewenstein, A. Sanpera, V. Ahufinger, B. Damski, A. Sen(De), and U. Sen, Adv. Phys. **56**, 243 (2007).

[46] M. Lewenstein, A. Sanpera, and V. Ahufinger, *Ultracold Atoms in Optical Lattices: Simulating Quantum Many-Body Systems* (Oxford University Press, Oxford, 2012).

[47] L.-M. Duan, E. Demler, and M. D. Lukin, Phys. Rev. Lett. **91**, 090402 (2003).

[48] L. Santos, M. A. Baranov, J. I. Cirac, H.-U. Everts, H. Fehrmann, and M. Lewenstein, Phys. Rev. Lett. **93**, 030601 (2004).

[49] B. Damski, H.-U. Everts, A. Honecker, H. Fehrmann, L. Santos, and M. Lewenstein, Phys. Rev. Lett. **95**, 060403 (2005).

[50] B. Damski, H. Fehrmann, H.-U. Everts, M. Baranov, L. Santos, and M. Lewenstein, Phys. Rev. A **72**, 053612 (2005).

[51] R. Schmied, T. Roscilde, V. Murg, D. Porras, and J. I. Cirac, New J. Phys. **10**, 045017 (2008).

[52] A. Eckardt, P. Hauke, P. Soltan-Panahi, C. Becker, K. Sengstock, and M. Lewenstein, Europhys. Lett. **89**, 10010 (2010).

[53] A. Eckardt and M. Holthaus, Phys. Rev. Lett. **101**, 245302 (2008).

[54] A. Zenesini, H. Lignier, D. Ciampini, O. Morsch, and E. Arimondo, Phys. Rev. Lett. **102**, 100403 (2009).

[55] N. Goldman, G. Juzeliunas, P. Ohberg, and I. B. Spielman, Rep. Prog. Phys. **77**, 126401 (2014).

[56] N. Goldman and J. Dalibard, Phys. Rev. X **4**, 031027 (2014).

[57] P. Hauke, T. Roscilde, V. Murg, J. I. Cirac, and R. Schmied, New J. Phys. **12**, 053036 (2010).

[58] P. Hauke, T. Roscilde, V. Murg, J. I. Cirac, and R. Schmied, New J. Phys. **13**, 075017 (2011).

[59] P. Hauke, Phys. Rev. B **87**, 014415 (2013).

[60] J. Struck, C. Ölschläger, R. L. Targat, P. Soltan-Panahi, A. Eckardt, M. Lewenstein, P. Windpassinger, and K. Sengstock, Science **333**, 996 (2011).

[61] J. Struck, C. Ölschläger, M. Weinberg, P. Hauke, J. Simonet, A. Eckardt, M. Lewenstein, K. Sengstock, and P. Windpassinger, Phys. Rev. Lett. **108**, 225304 (2012).

[62] P. Hauke, O. Tieleman, A. Celi, C. Ölschläger, J. Simonet, J. Struck, M. Weinberg, P. Windpassinger, K. Sengstock, M. Lewenstein, and A. Eckardt, Phys. Rev. Lett. **109**, 145301 (2012).

[63] J. Struck, M. Weinberg, C. Ölschläger, P. Windpassinger, J. Simonet, K. Sengstock, R. Höppner, P. Hauke, A. Eckardt, M. Lewenstein, and L. Mathey, Nat. Phys. **9**, 738 (2013).

[64] W. Nolting and A. Ramakanth, *Quantum Theory of Magnetism* (Springer-Verlag, Berlin, Heidelberg, 2009).

[65] J. H. Xu and C. S. Ting, Phys. Rev. B **43**, 6177 (1991).

[66] M. Takahashi, Phys. Rev. B **40**, 2494 (1989).

[67] F. J. Dyson, Phys. Rev. **102**, 1217 (1956).

[68] S. V. Maleev, Zh. Eksp. Teor. Fiz. **33**, 1010 (1957).

[69] S. V. Maleev, Sov. Phys.–JETP **6**, 776 (1958).

[70] A. W. Sandvik and C. J. Hamer, Phys. Rev. B **60**, 6588 (1999).

[71] F. Pollmann, A. M. Turner, E. Berg, and M. Oshikawa, Phys. Rev. B **81**, 064439 (2010).

[72] F. Kolley, S. Depenbrock, I. P. McCulloch, U. Schollwöck, and V. Alba, Phys. Rev. B **88**, 144426 (2013).

[73] P. W. Anderson, Phys. Rev. **86**, 694 (1952).

[74] B. Bernu, P. Lecheminant, C. Lhuillier, and L. Pierre, Phys. Rev. B **50**, 10048 (1994).

[75] M. Weinberg, C. Ölschläger, C. Sträter, S. Prelle, A. Eckardt, K. Sengstock, and J. Simonet, Phys. Rev. A **92**, 043621 (2015).